

# **Use of Functional Correlation Tensors for fMRI Monitoring of Neuroplasticity During Motor Learning**

**by**  
**Tory Olivia Frizzell**

B.Eng., University of Guelph, 2017

Thesis Submitted in Partial Fulfillment of the  
Requirements for the Degree of  
Master of Applied Science

in the  
School of Engineering Science  
Faculty of Applied Science

© Tory Olivia Frizzell 2020  
SIMON FRASER UNIVERSITY  
Summer 2020

Copyright in this work rests with the author. Please ensure that any reproduction or re-use is done in accordance with the relevant national copyright legislation.

# Approval

**Name:** Tory Frizzell

**Degree:** Master of Applied Science

**Title:** Use of Functional Correlation Tensors for fMRI  
Monitoring of Neuroplasticity During Motor  
Learning

**Examining Committee:** **Chair: Michael Sjoerdsma**  
Senior Lecturer

**Ryan D'Arcy**  
Senior Supervisor  
Professor

**Xiaowei Song**  
Supervisor  
Adjunct Professor  
Biomedical Physiology and Kinesiology

**Carlo Menon**  
Supervisor  
Professor

**Bonnie Gray**  
Internal Examiner  
Professor

**Date Defended/Approved:** May 11, 2020

## Ethics Statement

The author, whose name appears on the title page of this work, has obtained, for the research described in this work, either:

- a. human research ethics approval from the Simon Fraser University Office of Research Ethics

or

- b. advance approval of the animal care protocol from the University Animal Care Committee of Simon Fraser University

or has conducted the research

- c. as a co-investigator, collaborator, or research assistant in a research project approved in advance.

A copy of the approval letter has been filed with the Theses Office of the University Library at the time of submission of this thesis or project.

The original application for approval and letter of approval are filed with the relevant offices. Inquiries may be directed to those authorities.

Simon Fraser University Library  
Burnaby, British Columbia, Canada

Update Spring 2016

## Abstract

The development of Functional Correlation Tensors (FCT) is driving novel investigations into whole-brain functional magnetic resonance (fMRI) signal synchronicity. FCTs are mathematically analogous to the established structural diffusion modality. Unlike conventional fMRI analysis, FCTs examine functional signal independently of hemodynamic response assumptions. In this work participants trained on a motor task for two weeks with fMRI and diffusion scans collected at baseline and endpoint. Using only baseline data, a significant correlation was detected for the fractional anisotropy of the diffusion data with the signal synchronicity anisotropy of the FCT data. Previous work on this data detected white matter (WM) neuroplasticity in motor regions between baseline and endpoint. As FCT is sensitive to WM function, it was hypothesized that WM neuroplasticity could be further detected. Significant increases in signal synchronicity were detected in areas of motor task planning and execution. This represents the first instance of this novel methodology for identifying neuroplasticity.

**Keywords:** Functional magnetic resonance imaging; Motor learning; Functional correlation tensors; White matter, Neuroimaging; Blood oxygen level dependent

## Acknowledgements

So many people have contributed both directly and indirectly to the creation of this thesis. I would have never gotten this far without my incredible support network.

First, I would like to thank my senior supervisor, Dr. Ryan D'Arcy for your extraordinary support and guidance throughout my entire master's work. I would also like to thank my committee members, Dr. Xiaowei Song and Dr. Carlo Menon, for their invaluable role in my research.

I deeply appreciate the help and support of everyone who was part of the Neurotech and ImageTech teams and my broader academic circle.

My friends, who were there to offer support in many forms; their brains for scanning, coffee dates for commiserating, and patient (and repeated) explanations of Bayesian Statistics.

Finally, I would like to thank my parents and sister for all their love and support. And for the phone calls where I avoided answering questions about my thesis progress. Sorry you get a dedication in an Engineering Thesis instead of a fantasy novel like I promised when I was little.

# Table of Contents

<b>Approval .....</b>	<b>ii</b>
<b>Ethics Statement .....</b>	<b>iii</b>
<b>Abstract .....</b>	<b>iv</b>
<b>Acknowledgements.....</b>	<b>v</b>
<b>Table of Contents .....</b>	<b>vi</b>
<b>List of Tables .....</b>	<b>viii</b>
<b>List of Figures .....</b>	<b>ix</b>
<b>Chapter 1 Introduction .....</b>	<b>1</b>
<b>1.1. Overview .....</b>	<b>2</b>
<b>1.2. Technical Background .....</b>	<b>2</b>
1.2.1. Fourier Transform.....	2
1.2.2. Pearson's Correlation .....	3
<b>1.3. MRI.....</b>	<b>3</b>
1.3.1. Physical principles .....	4
1.3.2. BOLD fMRI .....	7
1.3.3. WM fMRI .....	8
1.3.4. Diffusion Weighted Imaging .....	10
<b>1.4. Functional Correlation Tensors.....</b>	<b>11</b>
1.4.1. FCT Computation .....	11
<b>1.5. Previous Work .....</b>	<b>16</b>
1.5.1. FCT Applications .....	16
1.5.2. Neuroplasticity .....	16
1.5.3. WM Neuroplasticity Analysis.....	18
<b>Chapter 2. Structural and Functional Comparison DTI and FCT.....</b>	<b>20</b>
<b>2.1. Abstract.....</b>	<b>20</b>
<b>2.2. Introduction .....</b>	<b>21</b>
<b>2.3. Methods .....</b>	<b>22</b>
2.3.1. Participants.....	22
2.3.2. Experimental design .....	23
2.3.3. Scan Procedure.....	24
2.3.4. MRI Acquisition.....	24
2.3.5. DTI Analysis .....	25
2.3.6. BOLD fMRI Preprocessing.....	25
2.3.7. FCT Analysis .....	26
2.3.8. Statistics.....	26
<b>2.4. Results .....</b>	<b>27</b>
<b>2.5. Discussion .....</b>	<b>28</b>
<b>2.6. Conclusion.....</b>	<b>31</b>
<b>Chapter 3. Functional Correlation Tensors Reveal Motor Learning in White Matter. ....</b>	<b>32</b>

<b>3.1. Abstract.....</b>	<b>32</b>
<b>3.2. Introduction .....</b>	<b>33</b>
<b>3.3. Methods .....</b>	<b>35</b>
3.3.1. Participants.....	35
3.3.2. Experimental Design.....	35
3.3.3. MRI Acquisition.....	36
3.3.4. DTI Analysis .....	36
3.3.5. fMRI preprocessing for FCT.....	37
3.3.6. FCT Analysis .....	37
<b>3.4. Results .....</b>	<b>38</b>
<b>3.5. Discussion .....</b>	<b>39</b>
<b>3.6. Conclusion.....</b>	<b>41</b>
 <b>Chapter 4. ....</b>	 <b>43</b>
<b>4.1. Limitations .....</b>	<b>45</b>
<b>4.2. Future Directions.....</b>	<b>47</b>
 <b>References.....</b>	 <b>49</b>
 <b>Appendix A. Functional Task.....</b>	 <b>57</b>
A.1 Task Requirements .....	57
A.2 fMRI Task Review .....	57
A.3 Task Development.....	59
 <b>Appendix B. Behavioural Analysis .....</b>	 <b>62</b>
 <b>Appendix C. Participant Principal Eigenvector DTI &amp; FCT Overlay .....</b>	 <b>63</b>
 <b>Appendix D. DTI and FCT 3D Spatial Correlation .....</b>	 <b>64</b>
 <b>Appendix E. Additional Figures.....</b>	 <b>67</b>
E.1 Individual Pearson's Correlation.....	67
E.2 Significant Voxel Timeseries Data.....	68

## List of Tables

Table 1: Scan breakdown and timing for all MRI acquisition.....	24
Table 2: Tissue FA differences for DTI and FCT. Intensity is a metric of average anisotropy .....	28
Table 3: ROI Cluster Information.....	38
Table 4: Left Hand FCT FA Baseline < Endpoint Group level difference cluster size and location .....	39
Table 5: Regions of high DTI FA (structural) and FCT FA (functional) correlation .....	65

## List of Figures

Figure 1: Precessing protons (red) in external magnetic field, with net longitudinal magnetization (yellow).....	5
Figure 2: Precessing protons (red) after application of RF pulse at resonance frequency, with net transverse magnetization (yellow) .....	5
Figure 3: Gradient example slice selection .....	6
Figure 4: Brain activity effect on BOLD signal.....	7
Figure 5: Block design and expected hemodynamic BOLD response with sequence TR of 2s .....	8
Figure 6: FCT computation overview.....	11
Figure 7: 2D Representation of the voxel of interest (red) and unit direction vectors to adjacent voxels (blue) .....	12
Figure 8: Representation of BOLD time series data for each voxel in 3x3x3 neighborhood and their corresponding correlation with the voxel of interest .....	12
Figure 9: A 2D representation of scaled correlation vectors to adjacent voxels with ellipse of best fit (left) and 3D tensor representation with defining orthogonal eigenvectors .....	13
Figure 10: 3D spatio-temporal correlation tensor.....	14
Figure 11: Resulting Tensor map .....	14
Figure 12: Representation of a 3x3x3 voxel patch and one of it's immediate neighbouring patches .....	15
Figure 13: Example Outputs of the FCT process.....	15
Figure 14: Average across significant internal capsule voxels for mean subtract BOLD signal. Baseline group average and standard deviation are plotted in orange and endpoint group average and standard deviation are plotted in blue. Stimulus block is from zero to twenty-four seconds. The standard deviation, i.e. variance, is much greater at baseline than endpoint.....	19
Figure 15: A – Group Average Structural DTI FA map, B – Group Average functional FCT FA map. Image A has been resampled to have the same resolution as image B. The SNR of image A is greatly superior as it is constructed from structural DTI whereas image B has is constructed from rapidly acquired functional images.....	27
Figure 16: Modality Comparison Participant example; A – DTI principal eigenvector (RGB colour coding for direction), B – FCT principal eigenvector (Purple-Orange-Magenta colour coding for direction), C – Overlaid DTI and FCT principal eigenvector to demonstrate alignment.....	28
Figure 17: Experimental design and training order for group 1 and group 2 participants	36
Figure 18: Left Hand task Endpoint > Baseline FCT FA ( $p < 0.05$ , FWE corrected). ROI Callosal Body. ....	38
Figure 19: Left Hand task Endpoint > Baseline FCT FA ( $p < 0.001$ ). Image 1: Cluster in the Right Anterior Corona Radiata. Image 2: Cluster in the Right Superior	

Corona Radiata. Image 3: Cluster in the Right Posterior Corona Radiata .....	39
Figure 20: Screenshot of participant completing the fine motor task.....	60
Figure 21: Screenshot of participant completing the gross motor task.....	60
Figure 22: DTI and FCT principal eigenvector masked to WM for all participants at baseline .....	63
Figure 23: Primary motor cortex (GM) correlation cluster. Region for motor control.....	65
Figure 24: Precuneus (GM) Correlation Cluster. Region for visuospatial processing and motor coordination .....	65
Figure 25: Primary motor cortex (GM) correlation cluster. Region for motor control.....	66
Figure 26: Precuneus (GM) Correlation Cluster. Region for visuospatial processing and motor coordination .....	66
Figure 27: Individual R-values for FCT FA maps compared to participant DTI FA maps for both the right and left hand.....	67
Figure 28: Average across significant corpus callosum voxels with subtracted mean BOLD signal intensity for baseline (orange) and endpoint (blue). Group level standard deviation plotted around timepoint BOLD signal intensity means. Time at zero seconds represents the stimulus onset time.....	68
Figure 29: Average across significant superior corona radiata voxels with subtracted mean BOLD signal intensity for baseline (orange) and endpoint (blue). Group level standard deviation plotted around timepoint BOLD signal intensity means. Time at zero seconds represents the stimulus onset time. ....	69

# Chapter 1

## Introduction

The development of Functional Correlation Tensors (FCT), a new analysis tool of fMRI signals, is enabling novel investigations into whole brain functional neural networks. FCTs have the potential to provide a quantitative metric of brain function and have been shown to be sensitive to white matter (WM) activity.

WM injuries and pathologies are a major cause of mortality and disability; despite this, WM function has been underrepresented in current research. There is a rapidly growing body of literature investigating WM fMRI activation seeking to address this gap; however, research regarding WM functional neuroplasticity remained unexplored. To investigate this, a novel motor learning paradigm was developed, and a previous work successfully detected functional neuroplasticity in WM motor tracts.

As such, it was postulated that there should be detectable measures of neuroplastic change in WM activity using FCT. The main objectives of this work were 2-fold. First, the comparison between FCT and brain structure was investigated by comparing the measured fractional anisotropy of the fMRI response with the corresponding structural fractional anisotropy. Secondly, FCT was used to investigate changes in WM neuroplasticity during a motor training task.

Two main hypotheses were formulated based on the objectives.

1. Significant correlation would exist between the structural DTI metrics and analogous functional FCT maps derived from motor BOLD fMRI activation
  - Specifically, it was expected that white matter would exhibit strong fractional anisotropy compared to gray matter as measured by both modalities
2. FCT can be sensitive to WM neuroplasticity and can detect an increase in fMRI BOLD signal synchronicity in areas related to motor task execution.
  - Specifically, increases were expected in the non-dominant (left) hand task, consistent with the behavioural results and previous work

FCTs have been mainly applied to resting state fMRI paradigms and their applications with respect to task based analyses have been limited. No previous literature was found

using FCTs on a motor task. Additionally, FCTs have never been used to detect plasticity prior to this investigation.

By improving the ability to visualize whole brain function, this research will hopefully help create a foundation for improving the evaluation of brain dysfunction. A better ability to characterize WM activation and plasticity has the potential to improve the understanding of dynamic brain connectivity and its role in WM pathologies. WM pathologies are related to many types of cognitive and physical pathologies such as stroke, dementia, and mobility disorders and WM integrity is an overall brain health metric that cannot be neglected [1]. WM injury and pathologies and other types of acquired brain injury are a major cause of increased mortality rates and continued dependency in patients [2]. As such they are a major health concern for millions of Canadians. This has a significant impact on patients and their caregivers and has socioeconomic ramifications on the community and healthcare resources.

## **1.1. Overview**

In this first chapter the foundational technical concepts needed for this thesis will be introduced, including magnetic resonance imaging (MRI) physics, Fourier transforms, and other key concepts. Chapter 2 is a modified version of a paper submitted to Frontiers in Neuroscience on the significant correspondence between structural diffusion metrics and functional correlation tensors (FCT). Chapter 3 is modified version of a paper prepared for submission to Nature Communication employing FCT as measure of motor learning in white matter (WM) function. The final chapter will be a general discussion of the thesis results and will explore future directions and caveats.

## **1.2. Technical Background**

### **1.2.1. Fourier Transform**

The Fourier Transform is a signal processing tool that allows for spatial or time signals to be decomposed into their frequency components. These spatial or time based signals can be constructed from an infinite sum of sinusoids. In the case of digital images, the 2D discrete grid of dimensions  $N$  by  $M$  in the spatial domain can be transformed into a

frequency domain representation with the same dimensions. Equation 1 gives the 2D Discrete Fourier Transform used for decomposing digital images.

$$F(u, v) = \frac{1}{NM} \sum_{n=0}^{N-1} \sum_{m=0}^{M-1} f(n, m) e^{-j2\pi(u\frac{n}{N} + v\frac{m}{M})} \quad (1)$$

The 2D Inverse Discrete Fourier Transform, shown in equation 2, allows for the spatial domain construction of a digital image from the frequency domain representation.

$$f(n, m) = \sum_{u=0}^{N-1} \sum_{v=0}^{M-1} F(u, v) e^{j2\pi(u\frac{n}{N} + v\frac{m}{M})} \quad (2)$$

The Fourier Transform has numerous applications in signal processing for smoothing, artefact removal, filtering, etc. In MRI, the 2D Inverse Discrete Fourier Transform is key for the construction of MR images from the detected frequency signals.

### 1.2.2. Pearson's Correlation

Pearson's Correlation is a commonly used measure of linear correlation between two metric variables. Values of the correlation coefficient range from -1 to 1. The closer the value of the Pearson's Correlation Coefficient is to 1, the stronger the correlation, with a value 0 meaning no correlation. Negative values indicated an inverse correlation. Equation 3 below gives the formula for computing the correlation coefficient for two variables, x and y. In this representation  $\bar{x}$  and  $\bar{y}$  are the respective means.

$$r_{xy} = \frac{\sum_{i=1}^n (x_i - \bar{x})(y_i - \bar{y})}{\sqrt{\sum_{i=1}^n (x_i - \bar{x})^2} \sqrt{\sum_{i=1}^n (y_i - \bar{y})^2}} \quad (3)$$

The Pearson's correlation coefficient has numerous uses in statistical analyses; one common application is image comparison where the coefficient is used a metric for disparity [3], [4].

## 1.3. MRI

Magnetic Resonance Imaging (MRI) is a non-invasive imaging modality with ability to create visualizations of the physiology and anatomy of the body. MRI is based on magnetic field gradients and the application of radio frequency pulses to acquire the signal for imaging. This gives MRI the advantage over other modalities such as CT

and PET that employ ionizing radiation. The applications of MRI are numerous; it often used for disease diagnosis and clinical and preclinical research.

### 1.3.1. Physical principles

#### *Nuclear Magnetic Resonance:*

The most important generator of the MRI signal is individual protons, that are also hydrogen atoms' nuclei. Hydrogen atoms are abundant in the human body, primarily in water and fat.

The protons have a charge and property called spin, that creates a magnetic dipole moment, making them vital for imaging. When the protons are subjects to a high external magnet field, as found in an MRI scanner, the protons will align themselves with this external field, either in a parallel (low energy state) or anti parallel direction (higher energy state). This generates a net magnetization parallel (or longitudinal) to the external magnetic field.

These protons will precess (or wobble) around the axis defined by the external magnetic field. The frequency of this precession is defined by the Larmor equation (equation 4) and is dictated by two factors; the strength of the external magnetic field ( $B_0$ ), and the gyromagnetic ratio ( $\gamma$ ) – an inherent property of the particle. For the hydrogen atoms, the gyromagnetic ratio is 42.58 MHz/T.

$$\omega_L = \gamma \times B_0 \quad (4)$$

The application of a radio frequency (RF) pulse at the same frequency of precession, also referred to as the resonance frequency, will transfer energy to the protons. This causes protons to jump to a higher energy state, increasing the number of high energy spin protons and causing phase coherence of the precession of the protons. This results in a net magnetization in the transverse plane. This process is visualized in figure 1 and 2.

When the RF signal is turned off the protons 'relax'; they return to their original state. This means that the transverse magnetization disappears, and the longitudinal magnetization increases back to its original value before the pulse.

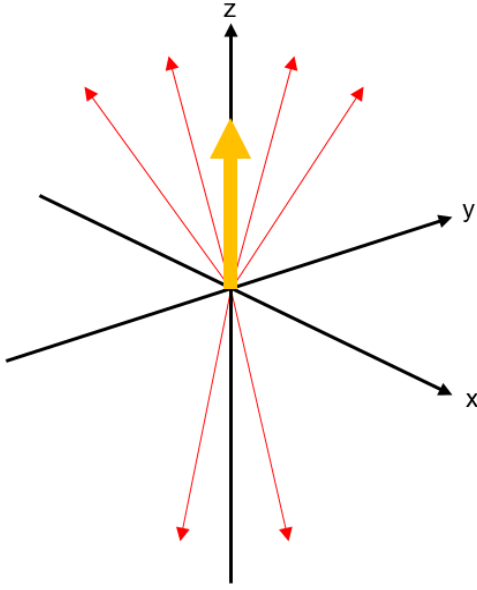


Figure 1: Precessing protons (red) in external magnetic field, with net longitudinal magnetization (yellow)

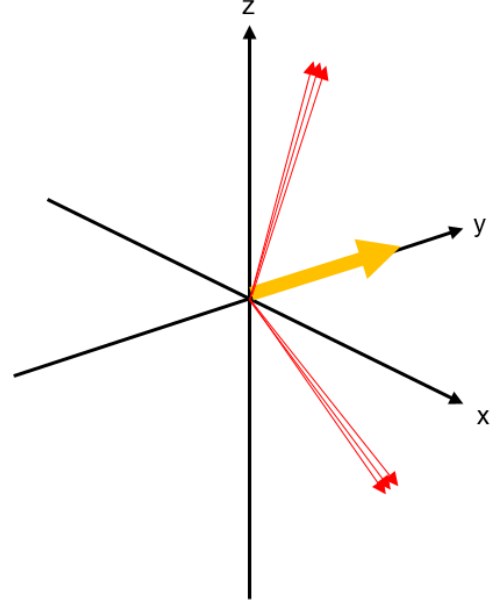


Figure 2: Precessing protons (red) after application of RF pulse at resonance frequency, with net transverse magnetization (yellow)

The relaxation is governed by the surrounding tissue structure (i.e. the lattice) and any local inhomogeneities in the magnetic field (i.e. susceptibility effects). The time constants of relaxation are T1, T2, and T2\*.

T1 is the longitudinal relaxation; the time constant for the protons to return to their original alignment in the magnetic field. i.e. equilibrium state. T1 is often referred to as Spin-Lattice relaxation. This is caused by the exchange in energy with the surrounding tissue. T1 is the decay constant the longitudinal magnetization. This relationship is shown in equation 5 where  $M_z(t)$  is the longitudinal magnetization at a given time  $t$ .

$$M_z(t) = B_0(1 - e^{-\frac{t}{T_1}}) \quad (5)$$

T2 is the time constant representing the time for the protons to lose their phase coherence due to their interactions with one another. T2 can also be referred to as transverse relaxation or Spin-Spin Relaxation.

T2\* is the effective time constant for the protons to lose their phase coherence, taking into account magnetic field inhomogeneities. This means that T2\* is the time constant for the signal decay. T2\* is the effective transverse relaxation.

### *Spatial Encoding*

Gradient coils in the MRI apply linearly varying magnetic fields in orthogonal directions to localize the signal (based on the proton precession frequency). An example of a gradient along the main magnetic field is represented in figure 3. Gradients vary the magnetic field slightly and therefore the precession frequency. This can be represented through a modified Larmor equation 6 presented below. Where  $r$  is the location (either in the x, y, or z direction) and  $G$  is the strength of the magnetic field of the gradient.

$$\omega_L(r) = \gamma \times [B_0 + G(r)] \quad (6)$$

In the z direction, parallel to the main magnetic field, the application of the gradient and RF pulse at the resonance frequency selectively excites the desired slice.

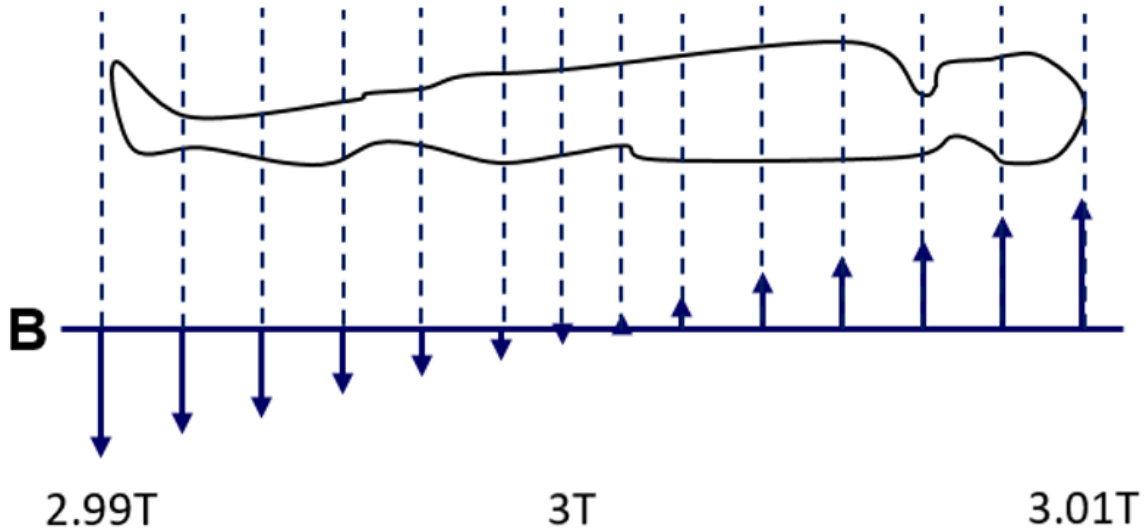


*Figure 3: Gradient example slice selection*

In the x direction, perpendicular to the main magnetic field, the application of the gradient labels the protons by varying their precession frequency. This is referred to as frequency encoding.

In the y direction, perpendicular to the main magnetic field, the application of the gradient labels the protons by varying their precession frequency. This is referred to as phase encoding.

The application of the RF pulse and the varying gradient coils allow the MR signal to be sampled repeatedly and determine the spatial frequencies that compose the image. The

collected spatial frequency information is stored in frequency domain i.e. k-space. The inverse Fourier transform of k-space gives the MRI image.

### 1.3.2. BOLD fMRI

Functional magnetic resonance imaging (fMRI) localizes brain activity based on cerebral hemodynamic changes [5]. The ability to map and understand brain function is a rapidly growing area of neurological research. While there are multiple ways to measure fMRI, the most common technique employs blood oxygen level dependent (BOLD) imaging which is summarized in figure 4.

During a task active state, corresponding brain areas increase oxygen consumption. This increased oxygen demand leads to a local increase in blood flow, a rise in oxyhemoglobin, and a relative decrease in deoxyhemoglobin concentration.

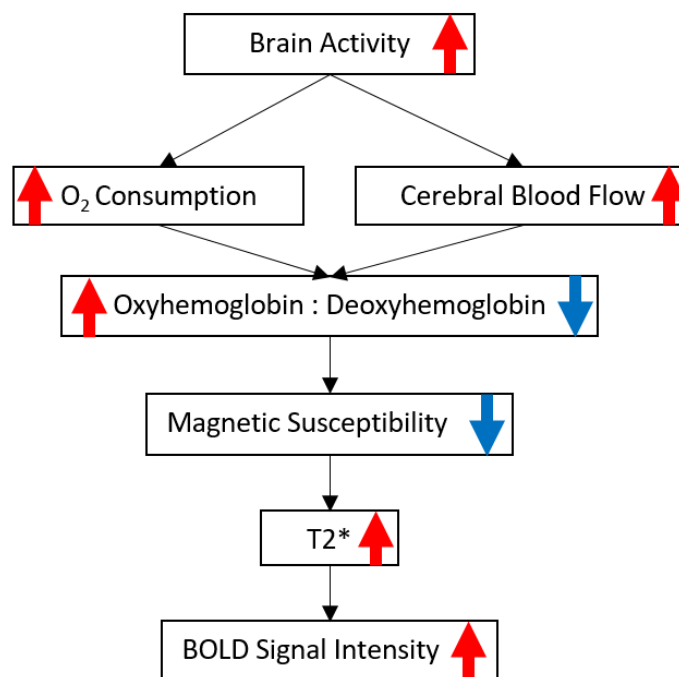


Figure 4: Brain activity effect on BOLD signal

Oxyhemoglobin is diamagnetic, while deoxyhemoglobin is paramagnetic. This change in concentration impacts the local magnetic field, and therefore the MRI signal. This allows for a time series acquisition of fluctuations in BOLD signal. BOLD fMRI measures the hemodynamic response of the metabolic demand of brain activity and is therefore an

indirect measure of neural activity. Figure 5 shows a simplified BOLD response following a block design stimulus presentation.

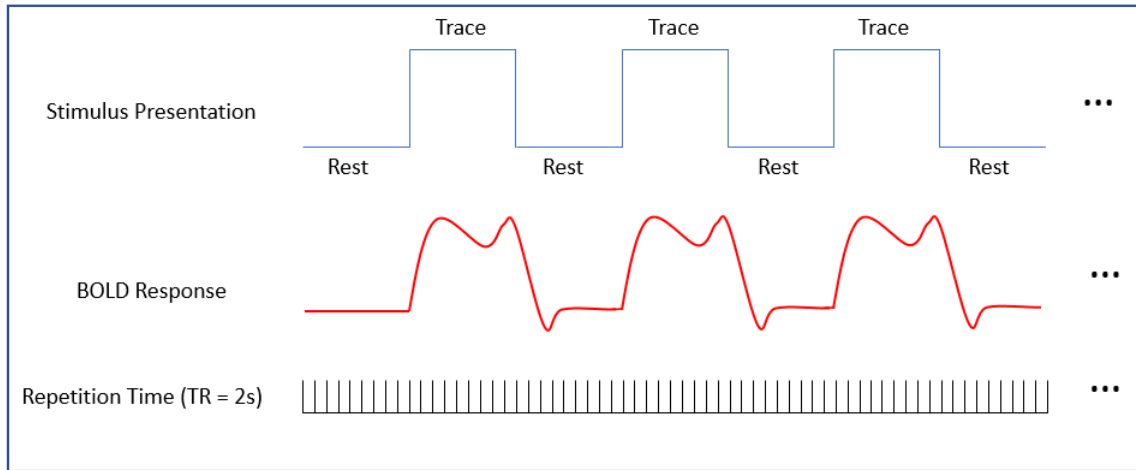


Figure 5: Block design and expected hemodynamic BOLD response with sequence TR of 2s

Traditionally, fMRI analysis employs a hemodynamic response function (HRF) that is a model of the expected signal fluctuations. The HRF is convolved with BOLD time series data to better detect localized brain activity. Given the relative uniformity of GM HRFs, they are robust and effective means for detecting activity in the cortical tissue. However, in recent years the use of an HRF has been shown to be somewhat limiting [6], [7] as optimal HRFs have been shown to vary throughout the brain [7], [8], and across a number of other parameters such as scanning time, tasks, and individuals [6]. Convolution with a time series signal that does not conform to assumptions of HRF onset and shape may limit the effectiveness of HRF driven analysis [6].

### 1.3.3. WM fMRI

The most common fMRI approach, based on BOLD contrast [9], has been widely accepted despite only having been optimized to detect the hemodynamic response to activity in the gray matter [9]–[11]. The brain is comprised of two approximately equal tissues; gray matter (GM) and WM [12]. WM tissue serves as the connecting architecture for the functional process of the brain and is a key indicator of brain wellness [13].

It was conventionally assumed that the 2-6 times lower blood flow and blood volume in white matter [14] would result in a lower signal that would preclude detection of a WM

BOLD contrast [15]. This has resulted in WM being often excluded from functional MRI research. As such, the role of WM in brain network activity and functional connections is largely unknown.

However, technological advances, such as the increasing availability of higher field MRI systems and specialized pulse sequences, have enabled the detection and characterization of WM fMRI activation for both resting state and task based experiments [15]–[17]. The use of high field strength MRI enabled the early WM BOLD investigations [16], [18]. Higher field strengths, such as 4T, have been shown to have an increased ability to detect WM BOLD and specialized sequences, such as asymmetric spin echo (ASE) have shown increased sensitivity to the comparatively small WM signal.

Once WM BOLD was found to be consistently detectable using specialized sequences and higher field MRIs several resting state and task-based studies successfully detected WM BOLD using standard sequences and field strengths [19], [20]. Numerous reports of activation in the corpus callosum have been published. Interhemispheric transfer tasks [8], [16], [21] that drive activation between hemispheres along WM tracts resulting in detectable signal. Sensory tasks, including tactile, taste, and visual stimuli have elicited activity in the corpus callosum and somatosensory WM bundles [22]–[24]. Activation in WM motor tracts, such as the internal capsule, has been detected during motor-based tasks, such as finger tapping tasks [25]. Previous work has taken care to rule out partial volume effects using conservative WM masks and co-localization with diffusion tensor imaging (DTI) tracts [20], [21]. However, WM activation continues to be frequently detected and then unreported. Mazerolle et al. 2019 [26] found that many peer reviewed fMRI journal papers displayed WM activation that went unmentioned.

More recently, advanced analyses have investigated the unique hemodynamic properties of WM. Sensitivity to WM BOLD signals has been improved by using a WM specific hemodynamic response function [8]. Li et al. (2019) [7] further confirmed this and found that the HRF may vary considerably throughout different areas of white matter tissue. This may be a contributing factor to the lack of detected WM activation in the literature, as GM HRFs are less sensitive to WM BOLD signal.

Given these advances in acquisition and analysis the ability to characterize WM activation is now generally accepted to not be artifactual [1], [17].

### 1.3.4. Diffusion Weighted Imaging

Diffusion Weighted Imaging (DWI) is an MRI scan type that uses anisotropic water diffusion in the brain to estimate the directionality of white matter fiber tracts.

When unrestricted, fluid particles will move randomly and they are equally likely to move in all directions, i.e. isotropically. In contrast, water diffusion is highly restricted in white matter, due to the directional nature of the fiber tracts. By measuring the water diffusion using an MRI, we can estimate the anisotropy of different areas of the brain and therefore estimate WM fiber structure.

Commonly, DWI is modelled through diffusion tensor imaging. A diffusion tensor is defined by 3 orthogonal eigenvectors and their corresponding eigenvalues. The principal water diffusion direction is defined by the largest eigenvalue  $\lambda_1$ , while  $\lambda_2$  and  $\lambda_3$  are the smaller eigenvalues.  $\lambda_1$  corresponds to the most probable direction of the fiber tract through that voxel. Based on DTI information probabilistic or deterministic fiber tracking can be calculated to get estimates of the major white matter tracts throughout the brain.

These tensors can be used to determine several measures relating to diffusion. The most relevant to this work are mean diffusivity and fractional anisotropy.

Mean diffusivity (MD) is a measure of the average water diffusion along each of the principal eigenvectors.

$$MD = \frac{\lambda_1 + \lambda_2 + \lambda_3}{3} \quad (7)$$

Fractional anisotropy (FA) is often the primary DWI measure used in research. DTI FA is a measure of the degree of water diffusion anisotropy. Gray matter areas of the brain have relatively isotropic water diffusion resulting in low values of DTI FA, while white matter has much higher values. In equation 8  $\hat{\lambda}$  represents DTI MD.

$$FA = \sqrt{\frac{3}{2}} \sqrt{\frac{(\lambda_1 - \hat{\lambda})^2 + (\lambda_2 - \hat{\lambda})^2 + (\lambda_3 - \hat{\lambda})^2}{\lambda_1^2 + \lambda_2^2 + \lambda_3^2}} \quad (8)$$

DTI FA can change over days/weeks of training and has been used in measuring WM structural neuroplasticity in a number of studies [10], [27], [28].

## 1.4. Functional Correlation Tensors

Recent studies have investigated analysis of fMRI signal using DTI-like tensor correlations to characterize the spatio-temporal activation. These functional correlation tensors allow a unique approach to analyzing whole brain functional synchronicity. The application of this mathematical analysis may allow a deeper understanding of the link between learning and the restructuring of the white matter of the brain [19].

### 1.4.1. FCT Computation

Figure 6 below gives a brief overview of the computation of functional correlation tensors. The preprocessed fMRI data and a corresponding tissue probability map are used to determine local correlation in the BOLD signal with surrounding voxels in order to calculate the principal correlation directions. Areas without functionally active tissue, such as the cerebral spinal fluid in the ventricle or in the skull, are not included in the analysis. The FCT calculation, which is explored in greater detail below, is computed voxel-wise throughout the brain based on the strength of local correlation with neighbouring voxels. These correlations are reduced to three primary directions and represented as a tensor. Visually, the tensor can be represented as an ellipsoid.

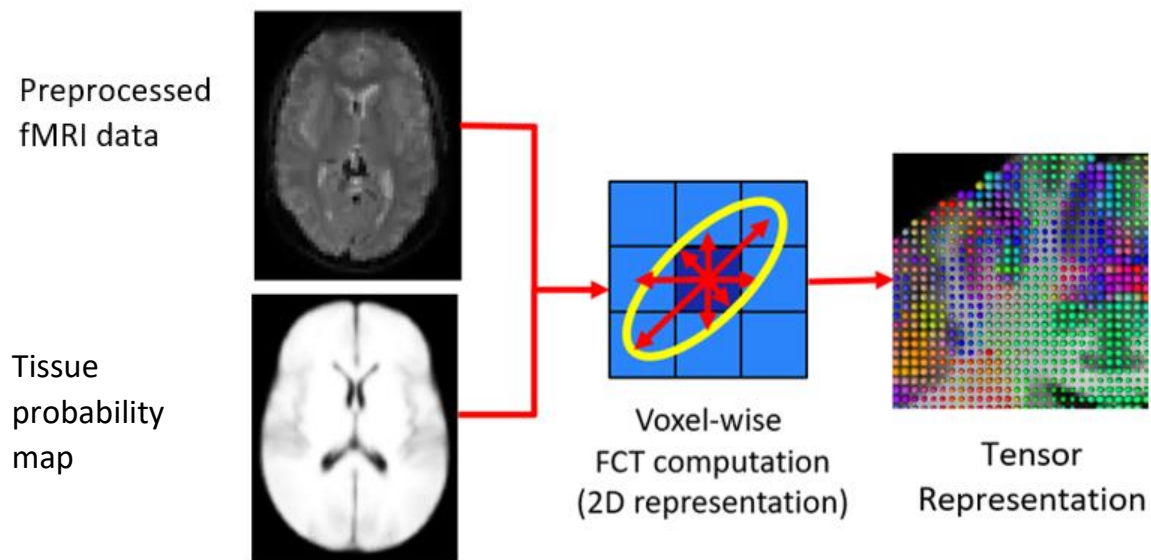


*Figure 6: FCT computation overview. Inputs to the computation: preprocessed fMRI data and a tissue probability map, taken from the MNI152 2mm T1WI standard. Using these inputs FCT is computed voxel-wise throughout the brain based on correlations with immediately adjacent voxels. A 2D representation of the correlation vectors is present here, though the actual computation is done in 3D. The output of the computation is a 3D tensor indicating directionality of BOLD correlation.*

For each voxel in 3-dimensional space, a set of unit vectors are defined that characterize the direction to each of the surrounding voxels. For a 2D example as seen in figure 7, this would be a set of 8 unit vectors, however, in 3D this would be a set of 26 unit vectors. The collection of adjacent voxels to the voxel of interest is referred to as a neighborhood.

Let  $n$  be the set of  $26 \times 3$  of unit directional vectors and  $n_{ij}$  be the  $1 \times 3$  unit vector between the voxels  $v_i$  and  $v_j$ . Where  $v_i$  is the voxel of interest (the center voxel) and  $v_j$  is the adjacent voxels.

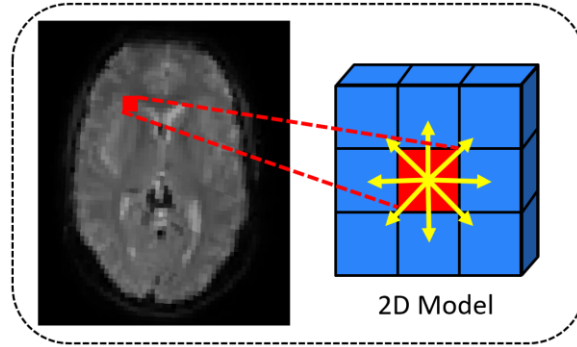


Figure 7: 2D Representation of the voxel of interest (red) and unit direction vectors to adjacent voxels (blue)

The time series BOLD data for each voxel is used to compute the squared Pearson's correlation coefficient corresponding to each voxel in the neighborhood. This gives a vector denoted as  $C$  with 26 entries representing each of the correlations. This computation is represented in figure 8.

	BOLD time series data	Pearson's Correlation
Voxel of interest		
Adjacent voxel #1		
...	...	
Adjacent voxel #26		

Figure 8: Representation of BOLD time series data for each voxel in  $3 \times 3 \times 3$  neighborhood and their corresponding correlation with the voxel of interest

For a 3D spatio-temporal correlation tensor  $T_{3 \times 3}$  (an upper right matrix of  $3 \times 3$  shown in equation 9, the correlation between two voxels, projected along the corresponding unit vector is given in equation 10.

$$T_{3 \times 3} = \begin{pmatrix} T_{xx} & T_{xy} & T_{xz} \\ T_{xy} & T_{yy} & T_{yz} \\ T_{xz} & T_{yz} & T_{zz} \end{pmatrix} \quad (9)$$

$$C_{ij} = n_{ij} T_{3 \times 3} n_{ij}^T \quad (10)$$

So, the tensor  $T_{3 \times 3}$  is the sum over the correlation all the adjacent voxels ( $j$ )

$$T_{3 \times 3} = \sum_{j=1}^{26} C_{ij} D_{ij} \quad (11)$$

Where  $D_{ij}$  is the dyadic tensor (equation 12) of the unit vectors where  $t$  denotes the transpose.

$$D_{ij} = n_{ij} n_{ij}^t = \begin{pmatrix} n_{ijx} \cdot n_{ijx} & n_{ijx} \cdot n_{ijy} & n_{ijx} \cdot n_{ijz} \\ n_{ijy} \cdot n_{ijx} & n_{ijy} \cdot n_{ijy} & n_{ijy} \cdot n_{ijz} \\ n_{ijz} \cdot n_{ijx} & n_{ijz} \cdot n_{ijy} & n_{ijz} \cdot n_{ijz} \end{pmatrix} \quad (12)$$

By taking the six free parameters of the tensor  $T_{3 \times 3}$  a 1 by 6 vector  $T_c$  can be obtained for each voxel in the 3D fMRI scan. The output of the FCT computation gives a 3D image with one volume for each entry in the  $T_c$  vector (i.e. 6 volumes).

Figure 9 below gives a 2D representation of correlation between voxels in a neighborhood. These correlation vectors are over-defined. 3 orthogonal eigenvectors and their corresponding eigenvalues are determined (using least squares) to define an ellipsoid of best fit. The largest eigenvalue ( $\lambda_1$ ) and the corresponding eigenvector indicates the primary direction of correlation for the voxel of interest with the adjacent voxels.  $\lambda_2$  and  $\lambda_3$  and their corresponding eigenvectors respectively define the secondary and tertiary directions of correlation. These orthogonal eigenvectors are defined by  $T_c$ , the 3D tensor (example shown on right in figure 9).

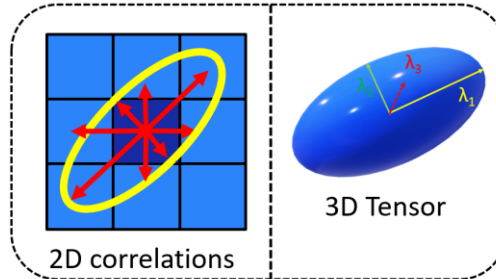


Figure 9: A 2D representation of scaled correlation vectors to adjacent voxels with ellipse of best fit (left) and 3D tensor representation with defining orthogonal eigenvectors

If we let  $M$  be the 26 by 6 design matrix for the six free parameters of the tensor for each of the 26 voxels, then we can represent the voxel correlation using equation 13 and the expanded matrix version using equation 14.

$$C = M.T_c \quad (13)$$

$$\underbrace{\begin{pmatrix} C_1 \\ C_2 \\ \dots \\ C_{26} \end{pmatrix}}_C = \underbrace{\begin{pmatrix} x_1^2 & 2x_1y_1 & 2x_1z_1 & y_1^2 & 2y_1z_1 & z_1^2 \\ x_2^2 & 2x_2y_2 & 2x_2z_2 & y_2^2 & 2y_2z_2 & z_2^2 \\ \dots & \dots & \dots & \dots & \dots & \dots \\ x_{26}^2 & 2x_{26}y_{26} & 2x_{26}z_{26} & y_{26}^2 & 2y_{26}z_{26} & z_{26}^2 \end{pmatrix}}_M \underbrace{\begin{pmatrix} T_1 \\ T_2 \\ \dots \\ T_6 \end{pmatrix}}_{T_c} \quad (14)$$

By applying the least squares equation, we can determine the best  $T_c$  for the voxel using equation 15.

$$T_c = (M^T.M)^{-1}M^TC \quad (15)$$

A 3D tensor is computed for each voxel in the gray and white matter (as defined by the tissue mask) giving an array of tensors seen in figure 10. An example of the tensors can be seen overlaid on a structural image in figure 11.

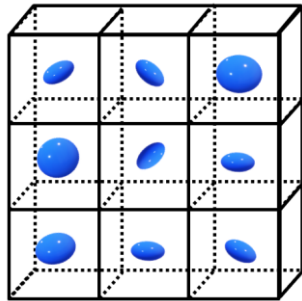


Figure 10: 3D spatio-temporal correlation tensor

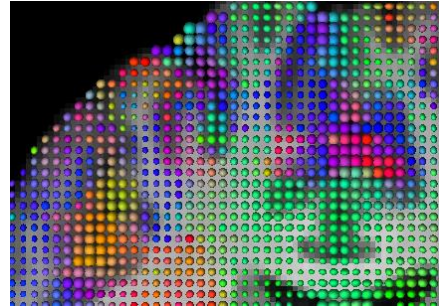


Figure 11: Resulting Tensor map

However, due to the sensitivity of fMRI data to noise, and the inability to use spatial smoothing to improve SNR, a method called patch based FCT was employed. A patch is a 3x3x3 group of neighboring voxels that are used for the FCT computation, rather than the immediate single layer of neighboring voxels. The correlation between each voxel in the patch of interest and its conjugate on the adjacent patch is computed. The average across all correlations is then used to represent the correlation between the center voxel

in the patch of interest and the adjacent voxel in the same unit direction as the computed adjacent patch. This has been shown to be more robust to noise than computing FCT for individual voxels [29], [30]. An illustration of a patch of interest and a single adjacent patch is presented in figure 12.

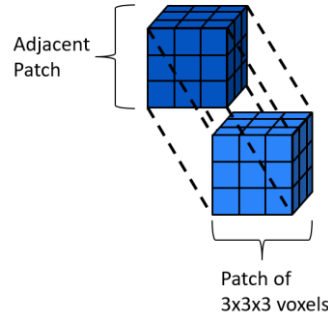


Figure 12: Representation of a 3x3x3 voxel patch and one of its immediate neighbouring patches

The final outputs of the FCT analysis give maps of Mean Diffusivity, Fractional Anisotropy, maps of each of the principal eigenvectors, and a tensor map as seen in figure 13. FCT mean diffusivity and fractional anisotropy are computed using the same equations as in DTI (equation 7 and equation 8 respectively). The V1 images represent the principal eigenvector for direction of correlation, V2 is a map of the secondary eigenvector, and V3 is the map of the tertiary eigenvector.

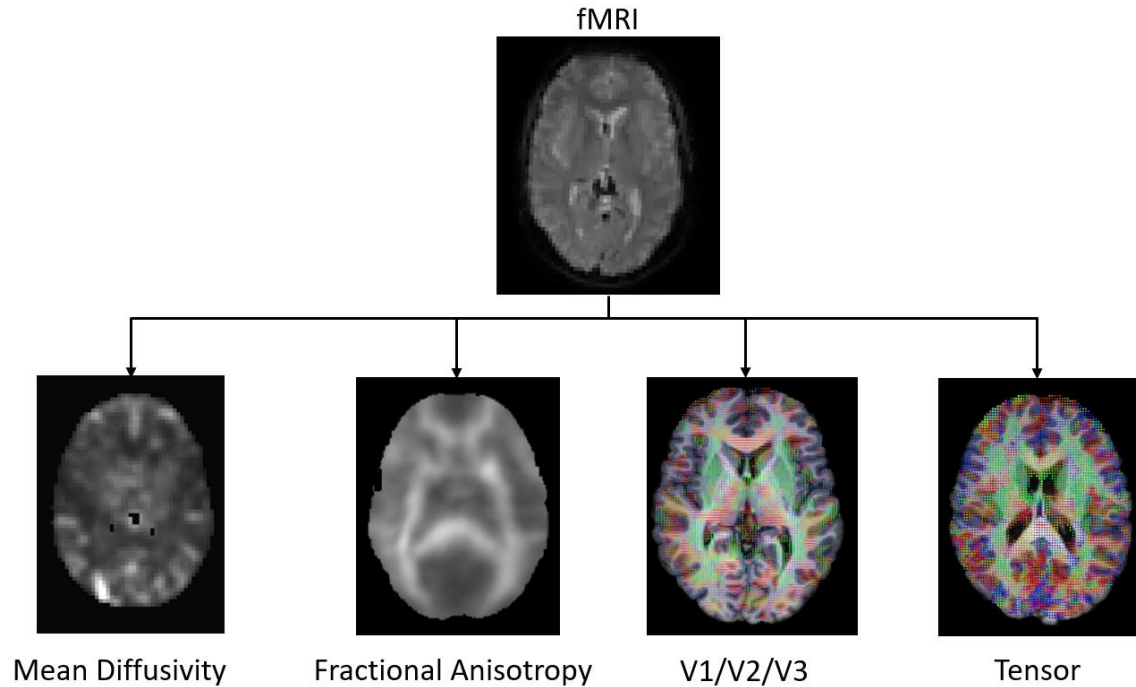


Figure 13: Example Outputs of the FCT process.

## **1.5. Previous Work**

### **1.5.1. FCT Applications**

Ding et al. (2013) initially develop FCT and applied it to resting state data in order to integrate the structural and functional aspects of brain activity in order to gain a better understanding of functional neural networks [19].

More recent work has investigated improving FCT. Zhang et al. (2017) used machine learning techniques to integrate DTI data to reduce sensitivity to noise [31]. The result was used to identify patients with Alzheimer's disease or mild cognitive impairment from normal subjects. Byeon et al. (2019) introduced the idea of enhancing FCT SNR using T1 image by structurally guiding the tractography [32]. They used these structurally guided WM specific FCTs to investigate used to identify biomarkers for obesity. Ding (2016) [33] used FCT to visualize more long-range WM tracts, similar to diffusion tractography for specific visual tracts. Importantly they raise concerns around computing FCTs at tissue boundaries.

To address this issue Zhou (2018) [29] employed FCTs to improve whole brain functional registration. This paper investigated computing WM and GM FCTs separately and then used a LDDMM to warp these two tissue-specific FCTs together to give a more accurate functional registration. This paper also introduced the idea of doing patch-based correlation sensors to improve FCT SNR without introducing false correlation.

### **1.5.2. Neuroplasticity**

Neuroplasticity is the brain's ability to restructure itself both physically and functionally in response to injury, learning, and rehabilitation [34]. Numerous studies have demonstrated a measurable change in fMRI activation as well as in DTI FA and DTI MD during longitudinal monitoring of motor and visuomotor learning tasks. One such study following six weeks of juggling training found significant changes in structural white matter before and after training. Daily training of the complex bimanual visuo-motor task showed increased in DTI FA in the WM underlying the intraparietal sulcus [27]. Cross sectional investigations corroborate this link between WM structure and function.

Proficiency in skills such as music, dance, and fine motor tasks have been linked with population difference in DTI FA [34]–[36]. Higher DTI FA in the corpus callosum was found to be higher in individuals with bimanual motor task performance [37]. A finger

tapping task training found significant fMRI activity changes in areas related to movement and motor coordination (motor cortex, basal ganglia, and cerebellum) [38].

Multiple works have investigated differences in neuroplasticity as function of dominant vs. non-dominant hand learning capabilities. A study trained participants on one of two finger tapping sequences for five days with left hand only. Differences in performance between trained sequence and the untrained sequence were tested for each hand during fMRI scans. Significant improvement in trained sequence was found to correspond to significant increases in stability of the activation pattern in the primary motor cortex for the trained hand only. The untrained (dominant) hand showed no significant differences [39].

Another finger tapping sequence task was trained for 4 weeks with the left hand. The results found an increase DTI FA in several white matter tracts associated with motor activity [28]. Specifically, an increase in DTI FA within the right CST was found [28]. The conjugate study using the same task showed a significantly lateralized difference in motor training for fMRI activity, between participants non-dominant and dominant hands [40].

Neuroplasticity also has essential applications in terms of rehabilitation. In cases of acquired brain injury, such as stroke or TBI there has been evidence of structural reorganization, but also changes in patterns of functional recruitment [41]. A case study of an individual with a severe traumatic brain injury reported significant functional changes corresponding to improved lower limb function while undergoing daily ambulatory rehabilitation [42]. Understanding neuroplasticity is key to guiding rehabilitation; a deeper comprehension of the brain changes occurring during recovery is key for developing more efficient treatment plans [41].

Other important considerations with measuring neuroplastic brain changes is the plateau effect during learning. The plateau effect for acquiring or honing skills means that training no longer has a measurable effect on performance. This is dependent on the complexity of the motor task being trained, for example a simple finger tapping task may be learned quickly, while a more complex task such as a dance may require a longer period of time to perfect [43]. There are also trade-off considerations when determining performance metrics. There is often a trade-off with motor task performance between speed and accuracy. These measurements are often inversely correlated meaning that

speed or accuracy as a single measure for performance is insufficient. Assessing a function of both metrics may provide a solution [43].

### 1.5.3. WM Neuroplasticity Analysis

Prior analysis of this data is being publish in Frontiers in Human Neuroscience.

**Frizzell, T.O.** & Grajauskas, L.A., Liu, C.C., Ghosh Hajra, S., Song, X., D'Arcy, R.C.N., (2020). White matter neuroplasticity: Motor learning activates the internal capsule and reduces hemodynamic response variability. *Frontiers in Human Neuroscience*. (Accepted pending revisions).

The data used in this thesis have been analyzed previously using a neuroscience approach to detect WM activation changes using a WM specific hemodynamic response function. Significant WM activation was detected during both baseline and endpoint in visual and motor regions of the brain. As expected, the behavioural results showed that participants improved significantly in terms of task execution with their non dominant hand but exhibited no significant improvement with their dominant hand.

A significant change in hemodynamic variability between group level baseline and endpoint scans for the non dominant (left) hand task only was detected in the internal capsule using a WM specific HRF dispersion derivative. The BOLD timeseries response in this significant cluster is present below in figure 14. As can be seen in this figure the baseline scans have a much greater variability, as visualized by the standard deviation in orange as compared to the endpoint signal variability in blue. This work represents the first detection of WM activity neuroplasticity in the literature.

Following these results, it was postulated that there should be detectable measures of neuroplastic change in WM activity using FCT.

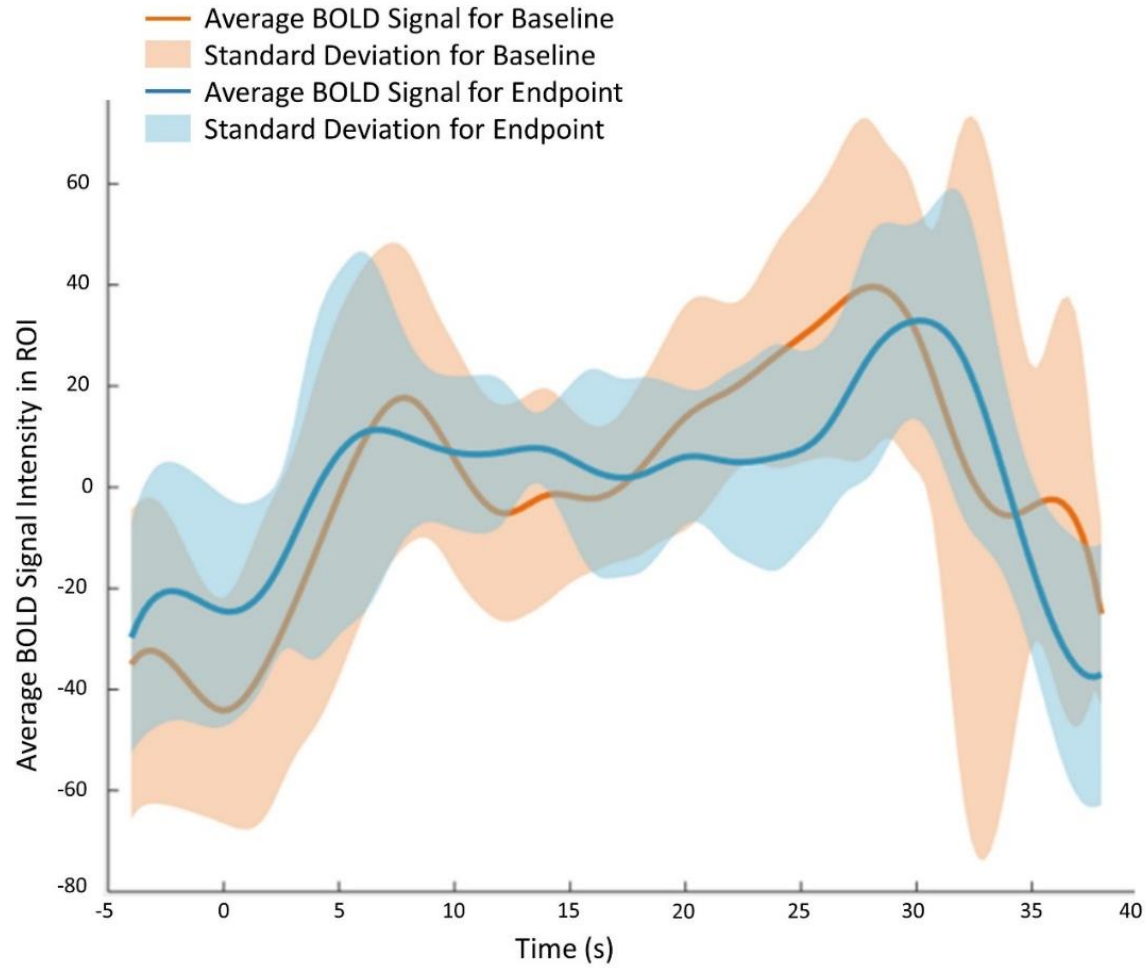


Figure 14: Average across significant internal capsule voxels for mean subtract BOLD signal. Baseline group average and standard deviation are plotted in orange and endpoint group average and standard deviation are plotted in blue. Stimulus block is from zero to twenty-four seconds. The standard deviation, i.e. variance, is much greater at baseline than endpoint.

## Chapter 2.

### Structural and Functional Comparison DTI and FCT

The contents of this chapter are submitted as an article in *Frontiers in Neuroscience*.

**Frizzell, T.O.**, Grajauskas, L.A., Liu, C.C., Ghosh Hajra, S., Song, X., D'Arcy, R.C.N., (2020). Functional Correlation Tensors Derived from BOLD fMRI Correspond with Structure Measured by DTI. *Frontiers in Neuroscience*. (Submitted)

#### 2.1. Abstract

There is a growing body of work seeking to develop a new fMRI BOLD analysis method called Functional Correlation Tensors. Similar to Diffusion Tensor Imaging, FCT measures local synchronization in terms of anisotropy. However, FCT specifically examines functional BOLD signal using DTI-like tensors independent of prior signal assumptions around the hemodynamic response function. FCT analyses include both GM and WM. BOLD fMRI activation in WM is being increasingly reported in both task-driven and resting-state studies. Accordingly, FCT represents a potentially important method for expanded characterization of WM activity as a critical aspect related to the functional architecture of the brain.

We investigated the relationship between brain structure and function with respect to the relationship between DTI and FCTs contrasted for a novel motor task. Participants performed a motor task during a BOLD fMRI, along with DTI data collected in the same session.

The results demonstrated a significant correlation between DTI and FCT results for WM. Specifically, DTI WM structural measures (fractional anisotropy and principal eigenvectors) were comparable to BOLD signal synchronicity for WM function in a task-driven experiment. The DTI/FCT correspondence is encouraging, as it opens up new avenues of investigation into whole brain functional analyses that includes the characterization of WM activation.

## 2.2. Introduction

Diffusion Tensor Imaging is an established method for examining WM fiber tracts [44]. DTI has advanced investigations into WM, but while the technique illuminates anatomical connections, it is incapable of investigating questions about functional activation. However, there is an inherent relationship between structure and function in the brain. Neural activity is intrinsically driven by the anatomical architecture and connections present in the brain structure [45]. As such, there should exist a relationship between structure measured by DTI and function as measured by fMRI BOLD contrast.

Recently, the development of a new tool for analyzing fMRI data, called Functional Correlation Tensors, is driving investigations into whole-brain functional connectomes [9]. FCTs use a mathematically similar approach to DTI to analyze local correlation in BOLD signal. Predominantly, FCTs have been applied to resting state data in order to gain a better understanding of functional neural networks. To accomplish this, hemodynamic fluctuations in each voxel are correlated with that of its adjacent neighbours to assess whether they are active in relative synchrony. This creates a matrix of 26 inter-voxel correlations for each voxel in 3D space that can be used to create a “local spatio-temporal correlation tensor” [9]. FCT analysis does not employ hemodynamic response functions or thresholding that may dampen weaker signals, such as those produced by WM activity. This makes it an ideal methodology for simultaneous analysis of WM and GM activity, as ideal HRFs have been shown to vary throughout the brain, particularly across WM structures [7]. In addition, FCTs can similarly be decomposed into metrics commonly used in DTI analyses such as fractional anisotropy, mean diffusivity, and principal eigenvectors. Owing to the relative ease of direct comparison within a common framework, FA and principal eigenvectors are particularly well aligned for initial comparisons between DTI and BOLD fMRI.

FCTs have been used for a variety of fMRI applications such as identifying obesity biomarkers in WM regions [32] and classifying Alzheimer’s and mild cognitive impairment patients from healthy controls [46]. An improved functional registration technique was also developed employing both WM and GM FCTs [47]. Recent work has investigated integrating structural information into FCT analyses, such as DTI or T1, to improve SNR [31], [32]. Additionally, FCTs have successfully been used to model long range WM tracts during resting state fMRI [33].

The evidence of BOLD signal in WM is increasingly supported by a growing body of work. To date, fMRI is largely dependent on assumptions about the underlying hemodynamic response function as a model in order to characterize functional activity. The most common fMRI approaches have focused on optimization of BOLD HRF for GM activity [7], [9]–[11], [48]. WM activity exhibits a different HRF with a lower peak and altered shape and therefore has been underrepresented in most functional neuroimaging research [5], [7], [13], [48]. However, advances in acquisition and analysis have improved the ability to characterize WM activation and it is now generally accepted to be detectable, and not necessarily artifactual [1], [17].

The advent of the new FCT technique presents a unique and critical opportunity to improve the characterization of white matter activation by directly linking structure and function, without relying on underlying assumptions about haemodynamic response functions. In order to integrate further, a basic comparison of relationship between DTI structure and fMRI function is a key first step. This can be readily evaluated within a task-driven experimental design, in which functional networks can be targeted *a priori*. For example, motor activation is well established in BOLD fMRI and can be utilized as a first step in DTI FCT comparison studies. Given the nature of the similarities in the mathematical approach, we hypothesized that the FA and principal eigenvectors will be significantly correlated between DTI and FCT maps derived from motor BOLD fMRI activation. Employing a targeted DTI-FCT motor activation analysis will enable new avenues of future WM activation investigations without requiring assumptions about haemodynamic response function characteristics.

## **2.3. Methods**

### **2.3.1. Participants**

Twelve healthy participants (seven female) were enrolled in this study. The mean age of the participants was  $25.8 \pm 3.7$  years (range 19 to 32). All participants were right hand dominant with normal or corrected to normal vision, and no history of neurological illness. The study was approved by the Research ethics boards of Simon Fraser University, the Fraser Health Authority, and the University of British Columbia. Written informed consent was provided by all participants prior to data collection.

Each participant completed the Edinburgh Handedness Questionnaire. This scale is a measure of the dominance or laterality of a participants right or left hand. The average score of the questionnaire was  $11.1 \pm 0.8$  (score of 12 meaning entirely right hand dominant).

Ethics approval was obtained by from the SFU REB. Participants were pre-screened for handedness, claustrophobia, normal vision or corrected to normal vision, pacemakers, metal implants, or other MRI incompatible objects, and recent tattoos. Participants who were pregnant or had a history of neurological disorders or brain injury were also excluded. Participants were screened by an MR technician before scanning for any MRI contraindications.

### **2.3.2. Experimental design**

The experimental design for this chapter represents a subsection of the larger study. In this analysis only the participants' baseline scans are included. Each participant was assessed using a diffusion weighted scan, a high resolution T1 weighted scan, and two fMRI task-based scans. The fMRI task was a visuo-motor task completed using an MRI compatible mouse. Details of the task can be found in Appendix A. The experiment used a block design: seven 24 second stimuli blocks alternating with eight jittered rest blocks. Two sets of images were acquired per participant; one with the task performed using their dominant (right) hand and one with their non-dominant (left) hand. The experimental paradigms have been presented in detail elsewhere in a previous work [17]. Briefly; participants were required to trace a path displayed on a screen as rapidly and accurately as possible. The paths consisted of sequential boxes on the screen controlled to total length and frequency of turns. Participants were able to view their progress and were not able to proceed with the task until every box has been passed over. Before scanning, each subject performed a brief practice of the task to ensure compliance. The task was displayed on a black background and rest blocks displayed a plain fixation cross. The stimulus was displayed on a screen outside of the bore and participants were able to view the task using a head coil mirror mount. DTI data were collected following the completion of the BOLD fMRI scans.

Participants each were scanned three times across two weeks following the described protocol, controlled to consistency factors such as time of day. Between scans

participants completed a short five-minute daily motor training regiment. For the purposes of this paper only the baseline scan data were used. The endpoint data will be included in Chapter 3.

### 2.3.3. Scan Procedure

Upon arrival participants completed demographics and the Edinburgh Handedness questionnaires. Written informed consent was given. Scan procedures were outlined, and participants were given a short tutorial and practice session to try each task on a laptop. After the tutorial participants were instructed to minimize head motion and use smooth movements during scans to improve image quality. Participants were screened a final time by the MR technician before entering the magnet.

The MRI compatible mouse and mouse pad were placed on in a comfortable position for the participant that allowed for easy movement. The stimulus was presented on a screen and a mirrored headset to allow for the participants to view the tasks.

The scans were allotted one-hour block (including set up). Table 1 below shows the individual scan time allotment. T1WI were used for registration of fMRI scans to a common template. Additionally, myelin water imaging scans were completed as part of a future investigation.

*Table 1: Scan breakdown and timing for all MRI acquisition*

Scan Type	# of scans	Time
T1WI – Anatomical Scan	1	5 minutes
Diffusion Tensor Imaging	1	7.5 minutes
fMRI Scans	4	6 minutes
Myelin Water Imaging	1	7 minutes
Total	7	43.5 minutes

### 2.3.4. MRI Acquisition

All MRI data were acquired with a 3 Tesla Philips INGENIA CX MRI scanner with a 32-channel dStream head coil. BOLD data were collected using a fast field echo, single

shot gradient echo type echo planar sequence. The acquisition parameters were as follows: TR = 2000ms, TE = 30 ms, and flip angle = 90°.

During the same session, DTI data were acquired using a single shot EPI sequence with 32 diffusion directions and b-value of 800. To provide co-registration of functional images, 3D high-resolution T1 weighted images were also acquired. Scan acquisition parameter were as follows: TR = 8.2 ms, TE = 3.7 ms, and flip angle = 8°.

### **2.3.5. DTI Analysis**

The DTI data were analyzed using FSL v6.0.0 Diffusion Toolkit following standard procedures [49]. The data were motion and eddy current corrected [50]. A binary brain mask was computed, and tensors were calculated using FSL's DTIFIT function. Track based spatial statistics (tbss) [51] were used to erode the DTI FA maps and zero the end slices to remove outliers. Next the DTI FA maps were registered to the FMRIB58\_FA 1mm standard space. An affine registration was then used to warp DTI FA maps to the MNI152 1mm standard space. The mean DTI FA and mean DTI FA mask were computed. The group mean DTI FA maps were down sampled from voxel size of 1mm<sup>3</sup> to 3mm<sup>3</sup> for computing correlation with BOLD FCT data.

The DTI principal eigenvector maps for each participant were registered to the MNI152 standard space using the DTI FA warp matrices computed during the previous processing step. The DTI principal eigenvector maps voxel size were similarly down sampled from 1mm<sup>3</sup> to 3mm<sup>3</sup>. MNI152 standard space WM masks were generated using the FAST function and used to mask the resulting principal eigenvector maps to WM for better visual analysis.

### **2.3.6. BOLD fMRI Preprocessing**

All fMRI data were preprocessed using FSL v.6.0.0 [49] BET and FEAT [52] functions following standard procedures. Brain extraction was done using the BET function [53] and motion correction was completed using the MCFLIRT function. The fMRI data were also slice time corrected and temporally high pass filtered with a cut-off of 100s. No spatial smoothing was used in order to avoid introducing false spatial-temporal correlation.

### 2.3.7. FCT Analysis

A GM and WM tissue probability map was computed for each participant using FSL FAST function. FCTs were computed using the preprocessed fMRI data and tissue probability map. A MATLAB script, adapted from Zhou et al (2018) existing code for patch-based FCT (<https://github.com/zyjshmlly/ts-PFCTs>) [47], was used to compute the spatio-temporal tensors, principal eigenvectors for  $\lambda_1$ ,  $\lambda_2$ , and  $\lambda_3$ , and FCT FA for each fMRI scan. This resulted in a set of right-hand task-based maps and left-hand task-based maps for each participant.

Left hand task data for all participants were subject to the following processing steps. Subsequently, right hand task data for all participants was also processed using the same methods. FSL's `tbss` [51] preprocessing and registration functions were used to register the resulting FCT FA maps to the FMRIB58\_FA 1mm standard space. An affine registration was then used to warp FCT FA maps to the MNI152 1mm standard space. An average FCT FA map for the task completed with each hand was computed across all participants' registered FCT FA images.

FCT principal eigenvector maps were registered to MNI152 standard space using FCT FA warp matrices computed in previous step. MNI152 standard space WM masks were generated using the FAST function and used to mask the principal eigenvector maps to WM for better visual analysis.

### 2.3.8. Statistics

Correlation analysis was computed using the group averaged DTI FA maps and FCT FA maps. The left-hand task average FCT FA map and right-hand task average FCT FA were individually compared against DTI data. The Pearson's correlation coefficient was computed across all nonzero voxels in the maps using MATLAB's correlation coefficient function. The significance threshold of the correlation was set at  $p < 0.05$ .

GM and WM tissue masks were computed for the standard template using FSL FAST function to compare FA for DTI and FCT measures. Differences in average intensity between tissues were computed using paired t-tests with Bonferroni correction for multiple comparisons for the DTI FA mean image, left-hand task FCT FA mean image, and right-hand task FCT FA mean image.

## 2.4. Results

FCTs were constructed for each participant for both their dominant and non-dominant hand. From this, the two key metrics used in the evaluation between DTI and FCT were the FA and the principal eigenvector direction. A comparison between the group average DTI FA and group average FCT FA can be found in figures 15. The mean FCT FA computed for all participants, after registration to the FMRIB standard template show clear similarities in terms of tissue patterns. The group mean FCT FA for the left-hand task only is shown for brevity, as there were no main differences when compared to the right-hand task FCT FA.

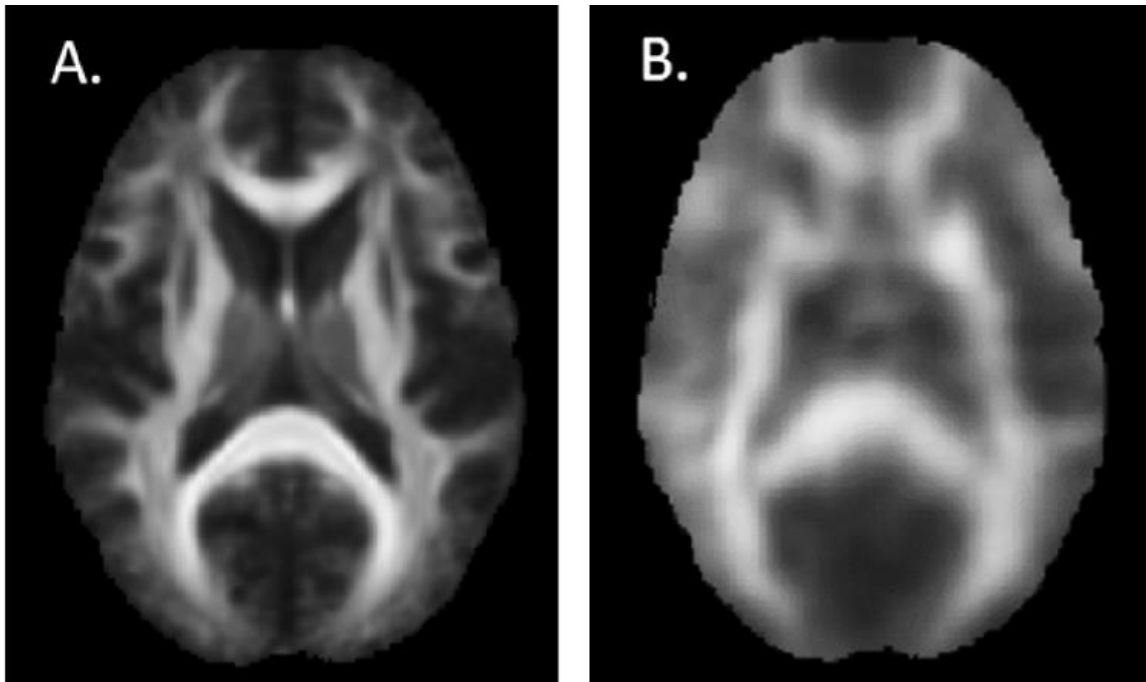


*Figure 15: A – Group Average Structural DTI FA map, B – Group Average functional FCT FA map. Image A has been resampled to have the same resolution as image B. The SNR of image A is greatly superior as it is constructed from structural DTI whereas image B has is constructed from rapidly acquired functional images.*

The correlation between the two modalities was computed to determine overall similarity. The correlation coefficient between DTI FA and FCT FA was  $R = 0.71$  ( $p < 10^{-16}$ ) for the right-hand task and  $R = 0.68$  ( $p < 10^{-16}$ ) for the left-hand task, indicating a medium (per Cohen's criterion) and significant correlation between the structural and fictional modalities. In addition, the tissue masked FCT FA maps showed that WM exhibited significantly greater fractional anisotropy than GM ( $p < 0.00001$ ) across both structural

and functional scan types. A summary of the tissue differences for FCT FA and DTI FA are presented in table 2.

*Table 2: Tissue FA differences for DTI and FCT. Intensity is a metric of average anisotropy*

	Average GM FA	Average WM FA	GM < WM statistics (Paired t-test)
DTI	0.1885 ± 0.0000331	0.3602 ± 0.000132	T = 71.80, p < 0.00001
FCT (LH)	0.1161 ± 0.000349	0.1443 ± 0.000304	T = 16.92, p < 0.00001
FCT (RH)	0.1196 ± 0.000468	0.1470 ± 0.000433	T = 16.26, p < 0.00001

Visual examination shows alignment of the WM principal eigenvector directions between DTI and FCT for a representative subject in Figure 16. Refer to the Appendix C, figure 22, for remaining participants. These principal eigenvectors have been masked to WM specifically, as GM signals are isotropic and therefore principal eigenvector direction is not a pertinent measure. In figure 16 the principal eigenvector direction of water diffusion (the DTI structural measure) is found in A, whereas B represents the direction of BOLD correlation synchronicity (FCT functional measure) and an overlay of both measures demonstrating the high degree of alignment is depicted in C.

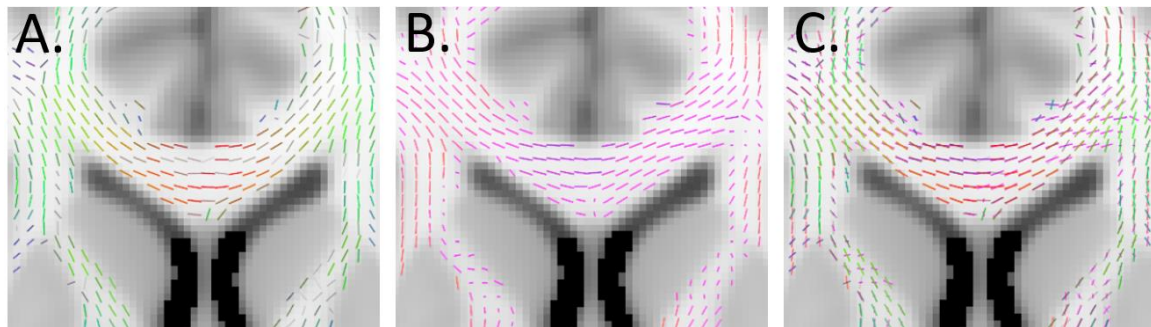


*Figure 16: Modality Comparison Participant example; A – DTI principal eigenvector (RGB colour coding for direction), B – FCT principal eigenvector (Purple-Orange-Magenta colour coding for direction), C – Overlaid DTI and FCT principal eigenvector to demonstrate alignment.*

## 2.5. Discussion

We hypothesized that the DTI measured WM fiber tracts would be consistent with functional structure as characterized by FCT. The results were consistent with this hypothesis, showing significant correlations for FA and principal eigenvector measures between DTI and FCT for WM (figure 16). Analyses of brain structure has long employed

DTI metrics such FA and tractography to investigate a variety of research and clinical applications. Likewise, BOLD fMRI represents the most commonly used MR measure of GM activity, with increasing applications in WM activity.

As predicted, the initial agreement results (Table 1) between DTI and FCT are limited in terms of visualization for GM isotropic patches because of the similarities between the three principal eigenvectors (or directions of correlation). In contrast, WM FCT FA intensities were significantly higher. The lower FCT FA in GM is consistent with the fact that the BOLD signal in the GM is highly synchronous with all of the immediate surrounding tissue. The visual similarities between DTI and FCT were consistent across FA and principal eigenvectors, but there were clear expected differences in SNR for FA maps. However, the mean DTI FA image is the average across images acquired through a relatively long scan (~7 mins) and therefore exhibits much higher SNR. Whereas, the FCT FA average image is constructed using conventional BOLD fMRI scans. The rapid, and relatively lower resolution, BOLD fMRI images are acquired with a TR of 2 seconds and not signal averaged. Therefore, FCT FA have a comparatively poor SNR, that further underscores the significance of comparable results observable in principal eigenvectors.

WM has been robustly detected [5], but the signal may frequently be missed or under reported due to lack of sensitivity of conventional analyses. Technological advances, such as the increasing availability of higher field (3T) MRI systems and parallel imaging, have enabled the detection and characterization of WM fMRI activation to be increased for both task based and resting state experiments [15]–[17]. DTI has been used to localize BOLD signal on key WM tracts connecting areas of GM activation [21]. This demonstrated that WM BOLD signal arose in the structural connection between functionally active GM regions.

FCT is relatively new, but it is emerging as potentially important approach to expanding WM fMRI studies. The key advantage for WM fMRI activation detection relates to long-standing questions around the ability to visualize activity along an entire WM tract. WM fMRI studies to date have localized activation clusters within a larger distributed structural tract. Various factors, related to both the underlying neurophysiology and biophysics variables, can be studied experimentally in terms of the relationship between conventional BOLD fMRI analyses, FCT, and DTI metrics. Functional changes in principal eigenvector maps represent a particularly useful variable of interest.

Current literature focuses on conventional hemodynamic response functions that have been optimized for GM BOLD activation, and consequently reduced sensitivity to WM BOLD signal [7], [48]. By comparison, the WM HRF appears to be more variable, reduced and significantly different in shape and temporal peak characteristics [7], [48]. WM specific HRFs have been shown to improve sensitivity of BOLD signal [48], [54]. Importantly, FCT analysis in the current study was independent of any HRF model/assumptions, that may circumnavigate the location specific differences in signal convolution. By identifying spatially correlated HRF responses within WM fibre tracts, FCT can be used to confirm WM BOLD activation and expand sensitivity through optimization studies [5], [7], [48].

There are several caveats in the current study. One key concern is that WM areas with low BOLD activity may be more susceptible to a lack of coherence between DTI and FCT principal eigenvectors and FA. Low BOLD activity would result in poor SNR in these areas, that may impact the accuracy of FCT FA and principal eigenvector computation. Areas of poor coherence may also be a result of the underlying structural architecture. For example, sharp turns in WM tracts, crossing fibers, and WM bundle size may impact the relationship between DTI voxel principal eigenvector directions and FCT voxel principal eigenvector directions. The weak magnetic signal propagation along WM tracts [55] may result in some detectable directionality of MR signal introducing an inflated positive correlation between the DTI and FCT. These considerations may introduce inaccuracies into the data, though they are unlikely to greatly artificially improve the significance of correlation detected between structure and function. Further studies are thus needed to better elucidate these differences.

While DTI and fMRI images are often collected together, the technique presented here opens a new avenue for the direct integration of functional and structural data. These results using fMRI task data confirm the existing literature on FCT tissue differences from resting state, demonstrating a brain structure modulated synchronicity in resting-state BOLD signal [9], [29], [33], [47]. This novel use of a motor task opens up the next analysis using FCT to identify evidence of motor learning. These results increase the accessibility of analyzing functional change along key WM tracts. To our knowledge no previous analysis has been able to do this.

## **2.6. Conclusion**

An intrinsic correspondence relates brain structure and function driving the hypothesis that standard DTI FA and principal eigenvector should exhibit a significant correlation with BOLD based FCT metrics. The FA and principal eigenvector results of DTI structural data were significantly correlated with FCT functional data. This finding supports the growing body of literature supporting WM BOLD fMRI activation, while removing constraints of HRF model assumptions, enabling the ability to characterize the wider scale functional architecture of the brain.

## Chapter 3.

# Functional Correlation Tensors Reveal Motor Learning in White matter

The contents of this chapter are being prepared for submission to Nature Communications.

**Frizzell, T.O.**, Grajauskas, L.A., Liu, C.C., Ghosh Hajra, S., Song, X., D'Arcy, R.C.N., (2020). Functional Correlation Tensors Reveal Motor Learning in White Matter. *Nature Communications*. (Submission in prep)

### 3.1. Abstract

The development of new MRI technique sensitive to WM neuroplasticity is a key advancement towards obtaining a complete depiction of the complex changes occurring in neural networks during learning. Participants trained on a manual motor learning task with both their non-dominant (left) and dominant (right) hands for a two week period. Functional MRI scans and performance metrics were acquired before and after the training period for the motor task completed with each hand. Previous investigations on these data detected significant changes in the BOLD response within WM tissue. Specifically, the internal capsule was the site of a significant decrease in the WM hemodynamic response function dispersion derivative and by extension BOLD signal variability. A rapidly growing body of work has shown that Functional Correlation Tensors are sensitive to WM activity. As such, we hypothesized that FCT can be sensitive to WM neuroplasticity and can detect increase in fMRI BOLD signal synchronicity in areas related to motor task execution. The changes were expected to be found during the non-dominant (left) hand task, consistent with the behavioural results and the previous work on WM HRFs. A novel increase in functional signal synchronicity was detected in the corpus callosum genu after training for the left hand task only. At lower significance thresholds, increases in signal synchronicity were also detected throughout the contralateral corona radiata.

### 3.2. Introduction

This work represents the development of a new detection method for WM functional neuroplasticity. Standard analyses methods do not have the ability to easily measure functional brain changes in areas of lower BOLD signal. An analysis technique detecting BOLD signal synchronicity rather than peak signal difference has proved effective at isolating WM functional adaptations due to motor training.

There is a rapidly growing body of literature investigating the brain's capacity for neuroplasticity. Neuroplasticity is the brain's ability to restructure itself both physically and functionally in response to injury, learning, and rehabilitation [34]. This research is key for exploring new potential avenues for improving recovery after events such as traumatic brain injury or stroke. Longitudinal monitoring is essential for detecting brain changes when acquiring a variety of basic or complex motor skills [28], [40]. Repetitive training is key for the long-term retention of ability. For this reason, numerous investigations into neuroplasticity have focused on repetitive training of motor learning tasks [27], [38], [39], [56].

Neuroplastic brain changes can be captured using various MRI scans such as DTI, fMRI, T1WI, and MWI. Numerous reports using these methods have found reorganization of motor areas, language, and somatosensory regions [57]. fMRI and DTI are well suited for analyzing motor learning in longitudinal studies [28], [40]. DTI, however, is the leading modality for investigating WM structural neuroplasticity. Specifically, fractional anisotropy and mean diffusivity (MD) have been used as key biomarkers of WM structure. DTI is very sensitive to WM microstructure, making it powerful for investigating structural changes during learning or after injury [41]. Wang et al. (2014) found increases in FA over a 2-3 week training period on a variety of spatial-visual motor tasks in the corona radiata, internal capsule, and corpus callosum [58].

Functional correlation tensors quantify local functional synchronicity using DTI-like tensors [9]. The construction of FCTs have been described in detail elsewhere [9], [29]. However, in brief, FCTs assess the correlation of BOLD signal fluctuation in adjacent voxels, or groups of voxels. This allows the construction of spatio-temporal correlation tensors, much like diffusion tensors, that can be represented with metrics of FCT fractional anisotropy, mean diffusivity, and principal eigenvectors.

WM tracts are structurally anisotropic and have also been shown to exhibit a corresponding anisotropy in the local correlation of hemodynamic signal [9], [29]. This has the potential to open a new avenue for investigating functional connections. Due to the low signal strength and comparatively lower SNR, approaching the analysis of WM function may be best accomplished using non-standard metrics. Whereas DTI has been commonly used to investigate structural WM integrity, FCT may be used to measure WM functional connections [9], [32], [33]. There have been several advancements for improving WM fMRI detection [7], [16], [48] and WM structural neuroplasticity [56], [58], [59], however, very little work exists to determine a robust method for analyzing WM functional neuroplasticity.

A visuo-motor training experiment was created, similar in structure to that of Reid et al. (2017) [28] and Sale et al. (2017) [40]. Participants trained for two weeks on a motor tracing task with both their non dominant and dominant hand. This dataset has been analyzed in previous work [54] that found that there was reduced variability in BOLD response in the internal capsule after motor learning. A significant difference in the dispersion derivative of a WM specific hemodynamic response function revealed group level changes in the right internal capsule during the left hand (non dominant) task [54]. There was no detected corresponding change for the hemodynamic response in the right hand. This followed the behavioural results, where group statistics detect a significant improvement in task execution for the left hand task exclusively. Additionally, no significant changes in WM BOLD activity levels were detected between baseline and endpoint using conventional analyses.

Based on the aforementioned motor learning effects detected in WM we conducted this study to further investigate this effect using FCT. This research will further investigate WM neuroplasticity to achieve an understanding of the relationship between motor training through significant differences in spatio-temporal correlation in the brain. We hypothesized that significant changes in FCT FA would be detected over the training period in areas related to motor learning. Specifically, it was expected that WM BOLD synchronicity would increase as a result of learning between baseline and endpoint in the contralateral motor areas for the left hand task but not the right hand task.

### **3.3. Methods**

#### **3.3.1. Participants**

The same twelve healthy participants (seven female) from Chapter 2 were used in this analysis.

#### **3.3.2. Experimental Design**

Each participant was scanned 3 times one week apart (controlled to consistency factors, such as time of day) using a repeat measure cross-over. Each scan comprised of a T1WI anatomical scan, diffusion tractography imaging, and two task-based BOLD fMRI images. After completing the baseline scan, participants completed two weeks of daily at-home training on the task for both the dominant and non-dominant hand. A midpoint and endpoint scan were completed after one week of at-home training and after the final day of at home training respectively. The midpoint scan will be included in future analysis and this paper deals exclusively with the baseline and endpoint data points. Figure 17 has the scanning and training schedule for the participants.

Each participant completed the visuo-motor task using an MRI compatible mouse. This task is described in more detail in Appendix A. The task was developed in PsychToolBox3 and used a block design; seven 24 second stimuli blocks alternating with eight jittered rest blocks. Two sets of images were acquired per participant; one set with the task performed using their dominant (right) hand and once with their non-dominant (left) hand. The task required the participants to trace a path displayed on a screen as rapidly and accurately as possible. The paths consisted of sequential boxes on the screen controlled to total length and frequency of turns. Participants were able to view their progress and were not able to proceed with the task until every box has been passed over. Before scanning, each subject performed a brief practice of the task to ensure compliance. Performance was based on speed and accuracy to give an overall score for each attempt.



Figure 17: Experimental design and training order for group 1 and group 2 participants

### 3.3.3. MRI Acquisition

All MRI data were acquired with a 3 T Philips INGENIA CX MRI scanner with a 32-channel dStream head coil. BOLD data were collected using an FFE single shot GRE-EPI sequence. The acquisition parameters were as follows TR = 2000ms, TE = 30 ms, and flip angle = 90°.

During the same session, DTI data were acquired using a single shot EPI sequence with 32 diffusion directions and b0 of 800. To provide co-registration of functional images, 3D high-resolution T1 weighted images were acquired using. Scan acquisition parameter were as follows TR = 8.2 ms, TE = 3.7 ms, and flip angle = 8°.

### 3.3.4. DTI Analysis

Following standard preprocessing procedures, the DTI data were analyzed using FSL v6.0.0 Diffusion Toolkit [49]. First the data were motion and eddy current corrected using FSL's eddy correction tool [50]. Next, using FSL's DTIFIT the DTI FA images were calculated, and a binary brain mask was computed [53]. Voxel-wise statistical analysis of the DTI FA data was carried out using Tract-Based Spatial Statistics (TBSS) [51]. All DTI FA data were registered to the standard space.

The mean DTI FA image was then fed into FSL's tract based spatial statistics skeletonization function to determine the mean DTI FA skeleton. All DTI FA maps are projected onto the mean DTI FA skeleton using a standard threshold of 0.2.

Significant group level changes in DTI FA were compared between baseline and endpoint. Group statistics were set up using FSL's FEAT Glm [52] function and computed using the randomise function with threshold free cluster enhancement, family wise error correction, and a significance threshold of  $p < 0.05$  (corrected).

### **3.3.5. fMRI preprocessing for FCT**

All fMRI data were preprocessed using FSL v.6.0.0 [49] following standard procedures using the FEAT function [52]. Data were brain extracted using FSL's BET function and motion corrected using the MCFLIRT function [53]. The fMRI data were then slice time corrected and temporally high pass filtered with a cut-off of 100s. Spatial smoothing was not applied to prevent any false spatial-temporal correlation.

### **3.3.6. FCT Analysis**

FCTs were computed using an adapted script from Zhou et al (2018) [29] MATLAB code. The preprocessed fMRI data for each scan and a tissue probability map were used to compute the FCT FA maps. Four sets of FCT FA maps were obtained; baseline right hand task maps, baseline left hand task maps, endpoint right hand task maps, and endpoint left hand task maps.

Voxel wise statistical analysis of the FCT FA data was carried out using TBSS [51]. All FCT FA data were registered to the standard space.

ROI analysis was computed on select WM regions as defined Julich Histological Atlas (JHA). The Corona Radiata, Internal capsule, and the body of the Corpus Callosum were used as ROIs for determining significant group level changes FCT FA between baseline and endpoint. Group statistics were set up using FSL's FEAT Glm [52] function and computed using the randomise function with threshold free cluster enhancement, family wise error correction, and a significance threshold of  $p < 0.05$  (corrected) for each of the ROIs.

Following positive detection in the Body of the Corpus Callosum, but not the Corona Radiata or Internal Capsule, whole brain group level changes were computed between baseline and endpoint at a lower threshold. Group statistics were computed using the randomise function with threshold free cluster enhancement, and a significance threshold of  $p < 0.001$  (uncorrected). Clusters smaller than 50 voxels were discarded. Cluster locations were identified using the JHU White Matter Labels. Probability of the peaks residing in WM vs. cortical tissue was recorded using the Harvard-Oxford Subcortical Structure Atlas.

### 3.4. Results

The body of the corpus callosum region of interest analysis revealed a significant cluster in the genu as seen in Figure 18. This cluster represents a location of increased FCT FA ( $p < 0.05$ , uncorrected) i.e. increase BOLD signal synchronicity after motor training shown in Figure 18. There was no significant changes detected for the right hand motor task in any of the region of interests (ROIs) for baseline < endpoint. Nor were there any significant DTI FA changes detected over the training period.

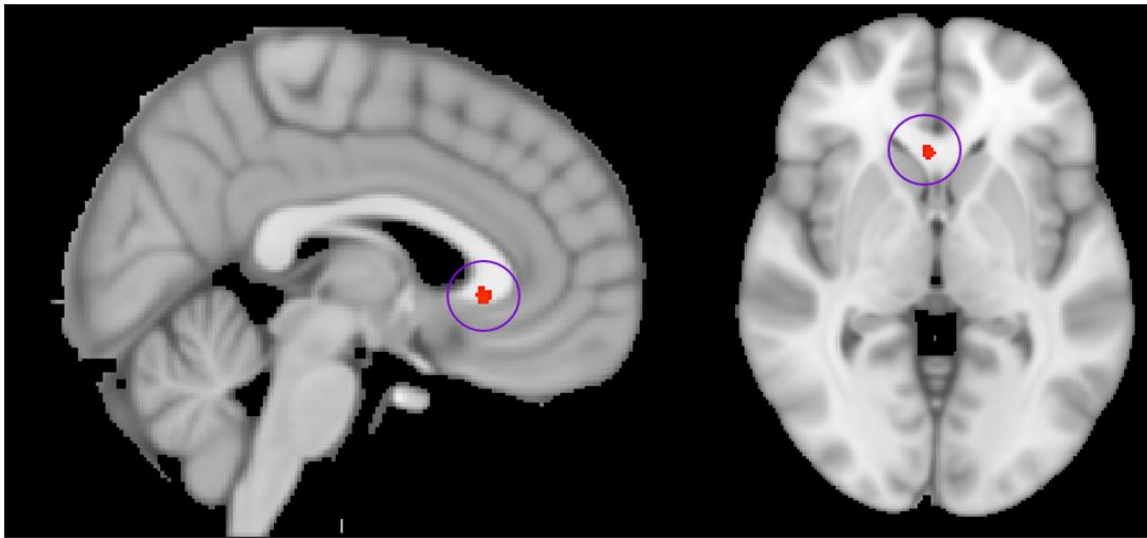


Figure 18: Left Hand task Endpoint > Baseline FCT FA ( $p < 0.05$ , FWE corrected). ROI Callosal Body.

Details of the significant cluster detected in body of the corpus callosum can be found in table 3 below. The location of this cluster was identified specifically as part of the corpus callosum genu.

Table 3: ROI Cluster Information

# of voxels	1-p max	X location	Y location	Z location	ROI
62	0.96	87	150	70	Corpus Callosum Body

Following the detection of significant group level FCT FA increases between baseline and endpoint a whole brain analysis was computed at a lower significance threshold ( $p < 0.001$ , uncorrected). This investigation found evidence of FCT FA increases in contralateral WM motor systems for the left-hand task. Similar to the results of the HRF

dispersion derivative decrease found in the previous analysis [54], there was no detectable change in FCT FA during the right-hand task even at  $p < 0.001$  (uncorrected). Table 4 shows the size and location of the main clusters of FCT FA change.

*Table 4: Left Hand FCT FA Baseline < Endpoint Group level difference cluster size and location*

# of Voxels	1-p max	x location	y location	z location	Atlas Region
70	0.999	63	162	71	Right Anterior Corona Radiata (100% WM)
62	1.000	63	89	102	Right Posterior Corona Radiata (100% WM)
51	1.000	58	105	99	Right Superior Corona Radiata (100% WM)

The clusters are located throughout the right corona radiata. These clusters can be seen in figure 19. A cluster was also detected in the genu of the corpus callosum, however, since this was reported in the ROI analysis, it was excluded from table 4 for simplicity.

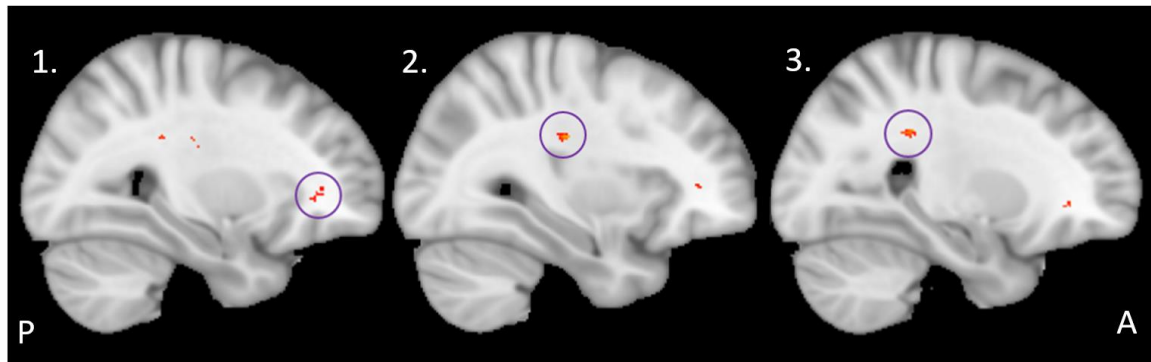


*Figure 19: Left Hand task Endpoint > Baseline FCT FA ( $p < 0.001$ ). Image 1: Cluster in the Right Anterior Corona Radiata. Image 2: Cluster in the Right Superior Corona Radiata. Image 3: Cluster in the Right Posterior Corona Radiata*

### 3.5. Discussion

These results confirm several key aspects of our hypothesis with respect to WM functional adaptation as a result of training on a fine motor task. We observed significant increases in FCT FA in WM ROIs between baseline and endpoint for the left hand task only. However, significant clusters of increased WM BOLD synchronicity were only detected in the corpus callosum genu and the corona radiata, but not the internal capsule. FCT detection of WM functional neuroplasticity represents a measure of functional change that standard analyses have not yet been able to detect.

The locations of the detected significant clusters in this study were consistent with previous works analyzing WM structural neuroplasticity during motor learning [28], [40], [58]. An overall increase in local synchronicity was measured in the corpus callosum genu and, at a lower significance threshold, throughout the corona radiata. These measures suggests that as motor learning occurs it drives an increase in BOLD signal synchronicity in corpus callosum genu. The corpus callosum genu is comprised of WM tracts connecting to the prefrontal cortex; an area known for synthesizing information and solving sensory-motor tasks [60]. The task the participants were training on incorporated several motor and sensory activities including visual stimulus, fine motor control, and tactile sensation from the fingers. The genu of the corpus callosum also represents a relatively common area of detected WM activation. In particular, previous studies have found activation in the genu during interhemispheric tasks like the Poffenberger task [12], [61]–[63].

Additionally, several areas of activation were found throughout areas of the right corona radiata. The corona radiata is made up of motor and sensory pathways between the brain stem and the cerebral cortex. The architecture and function of the corona radiata and the internal capsule are tightly coupled; the axons that form the corona radiata continue down through the posterior limb of the internal capsule [64].

This increased synchronicity in prefrontal cortex WM tracts and the corona radiata, coupled with the previous results detecting a reduction in hemodynamic variability in the internal capsule [54], suggests that there are several underlying changes resulting in motor learning. This result suggests that the changes occurring are highly complex and traditional analyses have failed to capture all of the nuances of motor learning driven functional brain changes.

It is unclear if the changes in WM HRF dispersion derivative and FCT FA increases are driven by the same underlying structural changes, or different, location specific, microstructure alterations. The measured decrease in functional HRF dispersion derivative may be related to the increased FCT FA, though given these changes were not detected in the same regions at significant thresholds, there may be many different responses occurring throughout the brain. If this is the case, the detected increase in local synchronicity is a previously uninvestigated facet of the complex changes occurring during motor training.

The detection of the clusters of significant FCT FA increase complement the existing body of literature that has managed to capture WM structural neuroplasticity using measures such as DTI FA. Diffusion tractography imaging has been used to localize WM BOLD signal on key WM tracts connecting areas of gray matter activation [21]. In addition, WM microstructure has shown plastic change with motor learning training [34], [40]. However, this work represents one of the first significant functional brain change measures for WM activity and, to our knowledge, the first significant measure of WM neuroplasticity using FCT.

There are several caveats to take into consideration when interpreting these results. First, the sample size of 12 participants is not large and thus limits statistical power. In future investigations a larger sample size may help detect more subtle functional and structural changes in the brain. Secondly, the clusters detected in the corona radiata are uncorrected for multiple comparisons. However, the conservative  $p < 0.001$  and cluster locations in the contralateral hemisphere to the hand completing the task strongly supports the validity of these results.

DTI FA has been shown to exhibit increases in many studies of neuroplasticity, however, there are also several works that found decreases in the metrics as a result of motor training [40]. These results vary from study to study and have been shown to be dependent on the task itself, the location of detected change, and the length of the training period [40]. The inconsistencies in reports of DTI FA changes are likely considered to be a result of the complexity of the underlying WM microstructure. In particular, it has been postulated that the inconsistency in DTI FA changes are a result of crossing fibers within a single voxel [59]. This complex relationship and comparatively small sample size may provide an explanation for the lack of detected DTI FA brain changes over the training period.

### **3.6. Conclusion**

Previous work detected changes in internal capsule during non-dominant hand motor learning as a reduction of BOLD signal variability. Additionally, FCT has been shown to be sensitive to detecting WM BOLD signal synchronicity. Therefore, FCT was expected to be able to detect WM functional neuroplasticity as a result of motor learning. The results of our investigation determined that FCT FA increased in key areas essential in

motor task planning and execution, i.e., the corpus callosum genu and the corona radiata. This study detected significant clusters of FCT FA increase, whereas the conventional HRF analyses failed to detect any group level differences between baseline and endpoint BOLD response. This novel result suggests that a complex network of changes, occurring throughout several brain regions, underlies neuroplastic motor processes.

## Chapter 4.

### Conclusions

This work had several novel features. First, this thesis represents the first use of FCTs on a motor task. FCT has primarily been used for resting state analyses, and this is one of the first investigations into the task-based applications of this analysis method. These results also capture one of the first functional brain change measures for WM activity and the first significant measure of neuroplasticity using FCT.

The intrinsic correspondence between brain structure and function was detectable using DTI FA and FCT FA. A significant correlation between BOLD signal synchronicity and underlying structure was detected in participants completing a motor task. This correspondence was confirmed based on DTI FA and FCT FA as well as with the principal eigenvectors. This means that WM exhibits highly anisotropic BOLD signal synchronicity and that BOLD signal is directional along white matter fiber tracts. This paves the way for a new analysis metric of whole brain task fMRI.

Additionally, using FCT we were able to detect signal in WM. Current literature purports that conventional hemodynamic response functions are optimized for GM BOLD response, and may dampen WM signal [7], [8]. The hemodynamic response in WM can be highly variable and significantly different than GM [7], [48]. The use of a WM specific HRF has been shown to improve sensitivity of BOLD signal generated by WM [48] [54], however, the analysis presented in this thesis does not require the use of an HRF at all that may circumnavigate the location specific differences in signal convolution. By identifying a logical, tissue correlated, BOLD response using FCT these results substantiate earlier reports of WM BOLD signal [7], [14], [48].

FCT was able to detect WM functional neuroplasticity as a result of motor learning. Previous work analyzing this data was able to successfully detect a significant group level decrease in the WM HRF dispersion derivative in the internal capsule. To further investigate the contrast before and after the two week motor training period, FCT FA was used to detect changes in BOLD signal synchronicity. Specifically, an increase was detected in the corpus callosum genu and the corona radiata. These areas are known to be key WM tracts involved in motor task planning and execution. Both the increases in

FCT FA and the previously noted decrease in BOLD signal variability were only found during the left-hand motor task. This is consistent with the behavioural response data where participants showed significant improvement in task execution during the left-hand task only, i.e. the non-dominant hand.

The overall behavioural scores were much higher in the dominant hand, but learning was found exclusively in the non dominant hand [65]. Both gross and fine motor training tasks had a significant effect on score improvement. It was theorized that this is a result of the similarities between the two training types. By practicing manipulating the mouse with their left hand during the gross motor training task, the participants gained skills that they were able to employ while completing the fine motor task. Given the rarity of using a computer mouse with the non dominant hand the gross motor training was sufficient to elicit a learning response. There was no effect found for training order so timepoint 2 was removed from the analysis for future study.

The detected timeseries BOLD responses for the corpus callosum and corona radiata, figures 28 and 29 in appendix C.2, do not closely resemble the canonical GM HRF. This atypical BOLD response exhibits a smaller magnitude that may be a result of the BOLD signal being spatially distributed along WM tracts. We postulate that a canonical double-gamma GM HRF is composed of the summation of multiple signal features; only some of which are present in WM tracts. Raw BOLD data are rich with information and the priors of a canonical HRF may mask key information.

There are many changes that underlie neuroplasticity for acquiring a new skill throughout a distributed neural network. These brain changes cannot all be detected using the same metrics and can only be detected by the application of several different analyses' methods.

FCT FA detected functional synchronicity changes that were distributed throughout the corona radiata and corpus callosum genu as presented in this work.

Increases in the magnitude of the BOLD response were detected in the GM, specifically in the inferior parietal lobules (IPL) in a previous analysis [65]. This region is key for visuospatial processing and plays a role in hand-eye coordination [66]. Specifically, the IPL retain the motor programs learned for hand-object coordination [66]. Bilateral IPL have been shown to work together with frontal motor regions to govern hand interactions

with objects [66], [67] such as the mouse used in this task. These changes were detectable using standard HRF analyses methods.

Additionally, prior work on this data detected decreases in the BOLD signal variability in the internal capsule by applying a WM specific HRF dispersion derivative analysis [54]. This WM region is responsible for relaying motor information to the spinal cord.

Structurally, the corona radiata tracts converge to the internal capsule. We hypothesize that these small synchronizations occurring throughout the corona radiata result in a confluence of the signals at the internal capsule where the information to coordinate the actual motor response is being conveyed. We postulate that the detection of each of these responses demonstrates the complex network of changes occurring during learning and highlights the necessity of a whole-brain analysis approach to neuroplasticity.

This may have important ramifications for measuring GM and WM connectivity as part of distributed neural networks. This novel motor learning paradigm has enabled detection of hereto uninvestigated metrics of BOLD signal synchronization as part of functional neuroplasticity. This synchronization may reflect a different way to track WM BOLD and could represent a fundamentally different but equally important functional measure than peak BOLD response.

As numerous studies have successfully elicited a WM BOLD signal, the next challenge is to optimize the ability to measure the response so that it can be reliably used as a brain health metric. A better understanding of neuroplasticity in the entire brain will help create the vital framework for stimulating learning and rehabilitation in response to brain injury.

## **4.1. Limitations**

Study specific limitations have been explored in their respective chapters, however, general fMRI and FCT considerations and task limitations are outlined below.

A common concern when detecting WM BOLD fMRI is that the signal is the results of partial volume effects. Previous literature has used conservative masking and co-localization with DTI [68] to ensure signal origin and the accumulating research has shown that WM fMRI can be consistently detected. However, by looking at the whole

brain in FCT we can see that WM has its own distinct fingerprint of activity. If the signal detected along GM tracts were a result of noise or partial volume effect, it would be unlikely to correlate so well with the anisotropy of the underlying brain structure.

Thus, while partial volume effects are unlikely to have artificially accounted for the WM signal, tissue boundary voxels are still a concern. The FCT FA measurements for voxels containing both tissue types will have limited significance and the use of patch-based FCT may exacerbate this issue.

There is not a measure for quality of MRI image registration, however, a lot of existing literature has highlighted the issues with functional registration. In addition, there is no FSL registration algorithm optimized for FCT. This may have led to reduced power in group level analysis due to poor FCT FA registration to the standard template. It has been proposed that a multi-channel large deformation diffeomorphic metric mapping (LDDMM) algorithm may provide a solution by treating WM and GM tensor maps as separate modalities [31]. In general, the issues with functional registration are more typical of resting state fMRI than task-based scans, however, this may provide a solution to the particular needs of FCT registration.

Another concern may be that the basis of the FCT correlation actually arises from structure rather than function. Traditional task fMRI analysis uses the difference in intensity from between task active and rest state. For a block design, this would be the difference between the on blocks with the off blocks as a comparison reference. FCT does not use this kind of difference analysis and questions may be raised regarding the similarities between FCT and DTI as results of the structural component of the fMRI data. However, if the resulting FCT correlation was strictly from structural correlation (i.e. high intensity WM, lower intensity GM) then we would only see variations in FCT FA at tissue boundaries and not the clear tissue differences in figure 15.

The task choice may have affected level of movement artifact. Though the task was piloted for standard head motion, this may be a particularly salient issue for FCT, as it is computing local correlation analysis. To date FCT has been primarily applied to resting state-fMRI, and while it has good potential applications for task-based fMRI, future analyses should consider employing tasks with less eye tracking and motion. While providing a sufficiently complex task to elicit lateralized fine motor learning, the

coordination of eye and hand movement caused an undesirable degree of head motion. Head motion is one of the most common and disruptive artifacts in neurological MRI scans [69]. Though there exists correction algorithms for motion artefact, minimizing movement during data collection will result in higher quality data. Typically, scans are discarded if the motion exceed 2mm of translation or 2° of rotation. While this was not found in the baseline and endpoint tracing scans used in the analysis in Chapters 3 and 4, it was detected in several other scans collected during this study.

## **4.2. Future Directions**

There are several avenues of investigation open to further this work. Primarily, a deeper investigation of the underlying timeseries hemodynamic response in the significant clusters of the corona radiata and corpus callosum should be conducted. Some preliminary findings have suggested that a signal frequency analysis of these key WM regions may elucidate the underlying signal. As these regions do not show a typical BOLD HRF, investigating the signal frequency during activation and rest may provide insight into WM activation and its role in neuroplasticity.

Additionally, future work should investigate the significant BOLD signal increase in the bilateral IPL with the DTI tractography between these regions. A better understanding of the underlying network responsible for motor neuroplasticity may be interrogated by isolating the relevant WM tracts analytically and comparing them to the locations of significant FCT FA increases.

Applying this study to populations with acquired brain injury may help this emerging technique become a useful clinical assessment tool. An objective measurement of the impacts of learning and rehabilitation on complex neural networks could be key in optimizing the recovery process.

Future development of FCT as an analysis method should investigate registration optimization as this is key for group level statistics. As mentioned in the limitations section, a major failing of FCT, and other fMRI analyses is functional registration. Comparing results between the existing FCT FA method and applying the LDDMM algorithm for GM and WM FCT registration or perhaps other machine learning techniques to improve comparison between participants.

FCT FA maps are insufficient for the FSL to compute tractography, however, there has been some work using machine learning to estimate FCT tractography [33]. A comparison between FCT tractography, particularly in the corticospinal tract, with DTI tractography could provide further evidence of the abilities of FCT to monitor WM activity and functional connectivity in motor areas of the brain. In addition, areas of the brain not in use for the task or other concurrent functions may not show good correlation in BOLD signal. Doing a tractography analysis for the specific visual and motor tracts may lead to a deeper understanding on the link between structure and function.

A longer study period may also open avenues in evaluating structural changes using DTI. Additionally, comparing changes in BOLD and FCT with myelin water imaging may garner a better understanding of underlying mechanisms behind the functional changes. Other structural modalities such as HARDI and MIX do not suffer from the same issues with crossing fiber determination as DTI. As such, they may be a better option for further investigating the structure-function relationship of the brain.

In future work similarities between the fine motor and gross motor tasks should be reduced. Developing a task with a better gross motor condition will enable a deeper analysis into the effect of motor training on neuroplasticity. A modified version of the task with a larger difference in training effects between the control condition and the task condition would allow for a better analysis of training effect and reduce the concern for carryover effects across training weeks. A modified task could be strictly motor to help isolate changes to more specific WM tracts and regions of interest as well as reduce head motion artefact.

Participant compliance was also an issue with the at home training component of the study. Four participants missed at least two training days that may have affected their performance. By not adhering to the training schedule these participants may have not achieved the same degree of neuroplastic learning and the associated improvements in score and FCT FA increase that they would have otherwise. Another limitation of this work was the hardware considerations. The MRI compatible mouse had very poor motion sensitivity that likely affected the scores of the participants as well as the skill transference from training to scan testing. Given significant improvements were still detected in task scores between baseline and endpoint, this is likely a minor concern. However, addressing these issues will help streamline the task for future analyses.

## References

- [1] I. Makedonov, S. E. Black, and B. J. MacIntosh, "BOLD fMRI in the White Matter as a Marker of Aging and Small Vessel Disease," *PLoS One*, vol. 8, no. 7, pp. 1–9, 2013.
- [2] E. L. Mazerolle, S. D. Beyea, J. R. Gawryluk, K. D. Brewer, C. V. Bowen, and R. C. N. D'Arcy, "Confirming white matter fMRI activation in the corpus callosum: Co-localization with DTI tractography," *Neuroimage*, vol. 50, no. 2, pp. 616–621, 2010.
- [3] A. M. Neto, A. Corrêa Victorino, I. Fantoni, D. E. Zampieri, J. V. Ferreira, and D. A. Lima, "Image Processing Using Pearson's Correlation Coefficient: Applications on Autonomous Robotics," 2013.
- [4] J. Adler and I. Parmryd, "Quantifying colocalization by correlation: The Pearson correlation coefficient is superior to the Mander's overlap coefficient," *Cytom. Part A*, vol. 77A, no. 8, pp. 733–742, Mar. 2010.
- [5] J. R. Gawryluk, E. L. Mazerolle, and R. C. N. D'Arcy, "Does functional MRI detect activation in white matter? A review of emerging evidence, issues, and future directions," *Front. Neurosci.*, vol. 8, p. 239, Aug. 2014.
- [6] P. N. Rosa, P. Figueiredo, and C. J. Silvestre, "On the distinguishability of HRF models in fMRI," *Front. Comput. Neurosci.*, vol. 9, no. MAY, May 2015.
- [7] M. Li, A. T. Newton, A. W. Anderson, Z. Ding, and J. C. Gore, "Characterization of the hemodynamic response function in white matter tracts for event-related fMRI," *Nat. Commun.*, vol. 10, no. 1, p. 1140, Dec. 2019.
- [8] M. J. Courtemanche, C. Sparrey, X. Song, A. MacKay, and R. C. N. D'Arcy, "Detecting white matter activity using conventional 3 Tesla fMRI: An evaluation of standard field strength and hemodynamic response function," *Neuroimage*, pp. 145–150, 2018.
- [9] Z. Ding, A. T. Newton, R. Xu, A. W. Anderson, V. L. Morgan, and J. C. Gore, "Spatio-temporal correlation tensors reveal functional structure in human brain,"

*PLoS One*, vol. 8, no. 12, 2013.

- [10] R. D. Fields, "Change in the Brain's White Matter: The role of the brain's white matter in active learning and memory may be underestimated," *Science* (80-. ), vol. 330, no. 6005, pp. 768–769, 2011.
- [11] W. S. Tae, N. Yakunina, T. S. Kim, S. S. Kim, and E. C. Nam, "Activation of auditory white matter tracts as revealed by functional magnetic resonance imaging," *Neuroradiology*, vol. 56, no. 7, pp. 597–605, 2014.
- [12] J. R. Gawryluk, E. L. Mazerolle, K. D. Brewer, S. D. Beyea, and R. C. N. D'Arcy, "Investigation of fMRI activation in the internal capsule," *BMC Neurosci.*, vol. 12, no. 1, p. 56, 2011.
- [13] L. M. Fraser, M. T. Stevens, S. D. Beyea, and R. C. N. D'Arcy, "White versus gray matter: fMRI hemodynamic responses show similar characteristics, but differ in peak amplitude," *BMC Neurosci.*, vol. 13, no. 1, 2012.
- [14] J. R. Gawryluk, E. L. Mazerolle, and R. C. N. D'Arcy, "Does functional MRI detect activation in white matter? A review of emerging evidence, issues, and future directions," *Front. Neurosci.*, vol. 8, no. 8 JUL, pp. 1–12, 2014.
- [15] K. L. Miller, S. M. Smith, P. Jezzard, G. C. Wiggins, and C. J. Wiggins, "Signal and noise characteristics of SSFP FMRI: A comparison with GRE at multiple field strengths," *Neuroimage*, vol. 37, no. 4, pp. 1227–1236, 2007.
- [16] J. R. Gawryluk, R. C. N. D'Arcy, E. L. Mazerolle, K. D. Brewer, and S. D. Beyea, "Functional mapping in the corpus callosum: A 4T fMRI study of white matter," *Neuroimage*, vol. 54, no. 1, pp. 10–15, 2011.
- [17] E. L. Mazerolle *et al.*, "Sensitivity to White Matter fMRI Activation Increases with Field Strength," *PLoS One*, vol. 8, no. 3, pp. 1–12, 2013.
- [18] J. R. Gawryluk, E. L. Mazerolle, S. D. Beyea, and R. C. N. D'Arcy, "Functional MRI activation in white matter during the Symbol Digit Modalities Test," *Front. Hum. Neurosci.*, vol. 8, no. August, pp. 1–8, 2014.
- [19] Z. Ding, A. T. Newton, R. Xu, A. W. Anderson, V. L. Morgan, and J. C. Gore,

“Spatio-temporal correlation tensors reveal functional structure in human brain,” *PLoS One*, vol. 8, no. 12, 2013.

- [20] J. R. Gawryluk, E. L. Mazerolle, and R. C. N. D’Arcy, “Does functional MRI detect activation in white matter? A review of emerging evidence, issues, and future directions,” *Front. Neurosci.*, vol. 8, no. 8 JUL, pp. 1–12, 2014.
- [21] E. L. Mazerolle, S. D. Beyea, J. R. Gawryluk, K. D. Brewer, C. V. Bowen, and R. C. N. D’Arcy, “Confirming white matter fMRI activation in the corpus callosum: Co-localization with DTI tractography,” *Neuroimage*, vol. 50, no. 2, pp. 616–621, 2010.
- [22] X. Wu *et al.*, “Functional connectivity and activity of white matter in somatosensory pathways under tactile stimulations,” *Neuroimage*, vol. 152, pp. 371–380, 2017.
- [23] M. Fabri and G. Polonara, “Functional topography of human corpus callosum: an FMRI mapping study.,” *Neural Plast.*, vol. 2013, p. 251308, 2013.
- [24] M. Fabri, “Functional topography of the corpus callosum investigated by DTI and fMRI,” *World J. Radiol.*, vol. 6, no. 12, p. 895, 2014.
- [25] J. R. Gawryluk, E. L. Mazerolle, K. D. Brewer, S. D. Beyea, and R. C. N. D’Arcy, “Investigation of fMRI activation in the internal capsule,” *BMC Neurosci.*, vol. 12, 2011.
- [26] E. L. Mazerolle, L. Ohlhauser, C. D. Mayo, A. Sheriff, and J. R. Gawryluk, “Evidence of Underreporting of White Matter fMRI Activation,” *J. Magn. Reson. Imaging*, vol. 24, pp. 2–3, 2019.
- [27] J. Scholz, M. C. Klein, T. E. J. Behrens, and H. Johansen-Berg, “Training induces changes in white-matter architecture,” *Nat. Neurosci.*, vol. 12, no. 11, p. 1370, 2009.
- [28] L. B. Reid, M. V. Sale, R. Cunnington, J. B. Mattingley, and S. E. Rose, “Brain changes following four weeks of unimanual motor training: Evidence from fMRI-guided diffusion MRI tractography,” *Hum. Brain Mapp.*, vol. 38, no. 9, pp. 4302–

4312, 2017.

- [29] Y. Zhou *et al.*, “Functional MRI registration with tissue-specific patch-based functional correlation tensors,” *Hum. Brain Mapp.*, vol. 39, no. 6, pp. 2303–2316, 2018.
- [30] Y. Zhou, P. Yap, H. Zhang, L. Zhang, Q. Feng, and D. Shen, “Improving Functional MRI Registration Using WHole-Brain Functional Correlation Tensors,” *Med Image Comput Comput Assist Interv.*, pp. 416–423, 2017.
- [31] L. Zhang, H. Zhang, X. Chen, Q. Wang, P. T. Yap, and D. Shen, “Learning-based structurally-guided construction of resting-state functional correlation tensors,” *Magn. Reson. Imaging*, vol. 43, pp. 110–121, 2017.
- [32] K. Byeon, B. yong Park, and H. Park, “Spatially guided functional correlation tensor: A new method to associate body mass index and white matter neuroimaging,” *Comput. Biol. Med.*, vol. 107, no. February, pp. 137–144, 2019.
- [33] Z. Ding *et al.*, “Visualizing functional pathways in the human brain using correlation tensors and magnetic resonance imaging,” *Magn. Reson. Imaging*, vol. 34, no. 1, pp. 8–17, 2016.
- [34] C. Sampaio-Baptista and H. Johansen-Berg, “White Matter Plasticity in the Adult Brain,” *Neuron*, vol. 96, no. 6, pp. 1239–1251, 2017.
- [35] S. L. Bengtsson, Z. Nagy, S. Skare, L. Forsman, H. Forssberg, and F. Ullén, “Extensive piano practicing has regionally specific effects on white matter development,” *Nat. Neurosci.*, vol. 8, no. 9, 2005.
- [36] G. C. Cannonieri, L. Bonilha, P. T. Fernandes, F. Cendes, and L. M. Li, “Practice and perfect: Length of training and structural brain changes in experienced typists,” *Neuroreport*, vol. 18, no. 10, pp. 1063–1066, Jul. 2007.
- [37] H. Johansen-Berg, V. Della-Maggiore, T. E. J. Behrens, S. M. Smith, and T. Paus, “Integrity of white matter in the corpus callosum correlates with bimanual co-ordination skills,” *Neuroimage*, vol. 36, no. SUPPL. 2, pp. 16–21, 2007.
- [38] L. G. Ungerleider *et al.*, “Imaging Brain Plasticity during Motor Skill Learning,”

*Neurobiol. Learn. Mem.*, vol. 78, pp. 861–868, 2002.

- [39] Y. Huang, Z. Zhen, Y. Song, Q. Zhu, S. Wang, and J. Liu, “Motor Training Increases the Stability of Activation Patterns in the Primary Motor Cortex,” *PLoS One*, vol. 8, no. 1, Jan. 2013.
- [40] M. V. Sale, L. B. Reid, L. Cocchi, A. M. Pagnozzi, S. E. Rose, and J. B. Mattingley, “Brain changes following four weeks of unimanual motor training: Evidence from behavior, neural stimulation, cortical thickness, and functional MRI,” *Hum. Brain Mapp.*, vol. 38, no. 9, pp. 4773–4787, 2017.
- [41] Z. Kou and A. Iraj, “Imaging brain plasticity after trauma,” *Neural Regen. Res.*, vol. 9, no. 7, pp. 693–700, 2014.
- [42] R. C. N. D’Arcy *et al.*, “Long-Term Motor Recovery After Severe Traumatic Brain Injury,” *J. Head Trauma Rehabil.*, vol. 31, no. 5, pp. E50–E58, 2016.
- [43] E. Dayan and L. G. Cohen, “Neuroplasticity subserving motor skill learning,” *Neuron*, vol. 72, no. 3, pp. 443–454, 2011.
- [44] D. G. Taylor and M. C. Bushell, “The spatial mapping of translational diffusion coefficients by the NMR imaging technique,” 1985.
- [45] V. Pernice, B. Staude, S. Cardanobile, and S. Rotter, “How Structure Determines Correlations in Neuronal Networks,” *PLoS Comput Biol*, vol. 7, no. 5, p. 1002059, 2011.
- [46] X. Chen, H. Zhang, L. Zhang, C. Shen, S. W. Lee, and D. Shen, “Extraction of dynamic functional connectivity from brain grey matter and white matter for MCI classification,” *Hum. Brain Mapp.*, vol. 38, no. 10, pp. 5019–5034, 2017.
- [47] Y. Zhou, P.-T. Yap, H. Zhang, L. Zhang, Q. Feng, and D. Shen, “Improving Functional MRI Registration Using Whole-Brain Functional Correlation Tensors,” *Med Image Comput Comput Assist Interv.*, vol. 2, pp. 108–115, 2017.
- [48] M. Courtemanche, C. Sparrey, X. Song, A. MacKay, and R. C. N. D’Arcy, “Detecting white matter activity using conventional 3 Tesla fMRI: An evaluation of standard field strength and hemodynamic response function,” *Neuroimage*, vol.

169, pp. 145–150, 2018.

- [49] S. M. Smith *et al.*, “Advances in Functional and Structural MR Image Analysis and Implementation as FSL Technical Report TR04SS2,” 2004.
- [50] J. L. R. Andersson and S. N. Sotiropoulos, “An integrated approach to correction for off-resonance effects and subject movement in diffusion MR imaging,” *Neuroimage*, vol. 125, no. 2016, pp. 1063–1078, 2015.
- [51] S. M. Smith *et al.*, “Tract-based spatial statistics: Voxelwise analysis of multi-subject diffusion data,” *Neuroimage*, vol. 31, no. 2006, pp. 1487–1505, 2006.
- [52] M. W. Woolrich, B. D. Ripley, M. Brady, and S. M. Smith, “Temporal Autocorrelation in Univariate Linear Modeling of FMRI Data,” *Neuroimage*, vol. 14, no. 2001, pp. 1370–1386, 2001.
- [53] S. M. Smith, “Fast Robust Automated Brain Extraction,” *Hum. Brain Mapp.*, vol. 17, pp. 143–155, 2002.
- [54] T. Frizzell, L. A. Grajauskas, C. C. Liu, S. Ghosh Hajra, X. Song, and R. C. N. D’Arcy, “White matter neuroplasticity: Motor learning activates the internal capsule and reduces hemodynamic response variability,” *Frontiers Hum. Neurosci.* (Manuscript Submitt. Publ., 2019.
- [55] P. A. Bandettini, N. Petridou, and J. Bodurka, “Direct Detection of Neuronal Activity with MRI: Fantasy, Possibility, or Reality?,” *Appl. Magn. Reson*, vol. 29, pp. 65–88, 2005.
- [56] B. Lakhani *et al.*, “Motor Skill Acquisition Promotes Human Brain Myelin Plasticity,” *Neural Plast.*, vol. 2016, pp. 1–7, 2016.
- [57] M. Staudt, “Brain Plasticity Following Early life Brain Injury: Insights from Neuroimaging,” *Semin. Perinatol.*, vol. 34, no. 1, pp. 87–92, 2010.
- [58] X. Wang, M. Casadio, K. A. Weber II, F. A. Mussa-Ivaldi, and T. B. Parrish, “White matter microstructure changes induced by motor skill learning utilizing a body machine interface,” *Neuroimage*, vol. 88, pp. 32–40, 2014.

- [59] M. Taubert *et al.*, “Dynamic properties of human brain structure: Learning-related changes in cortical areas and associated fiber connections,” *J. Neurosci.*, vol. 30, no. 35, pp. 11670–11677, Sep. 2010.
- [60] F. H. Chowdhury *et al.*, “White fiber dissection of brain: Safety of different commonly used transcortical microsurgical approaches to ventricles in relation to damage of the internal capsule and other white fiber tract: A cadaveric study,” *Neurosurg. Q.*, vol. 24, no. 1, pp. 9–17, Feb. 2014.
- [61] M. Tettamanti *et al.*, “Interhemispheric Transmission of Visuomotor Information in Humans: fMRI Evidence,” 2002.
- [62] K. Omura, T. Tsukamoto, Y. Kotani, Y. Ohgami, M. Minami, and Y. Inoue, “Different mechanisms involved in interhemispheric transfer of visuomotor information,” *Neuroreport*, vol. 15, no. 18, pp. 2707–2711, 2004.
- [63] B. Weber *et al.*, “Attention and Interhemispheric Transfer: A Behavioral and f MRI Study.”
- [64] E. K. Miller, D. J. Freedman, and J. D. Wallis, “The prefrontal cortex: Categories, concepts and cognition,” in *Philosophical Transactions of the Royal Society B: Biological Sciences*, 2002, vol. 357, no. 1424, pp. 1123–1136.
- [65] L. A. Grajauskas, “Detection of Motor-Learning Related Neuroplasticity in White Matter using Functional MRI techniques,” Simon Fraser University (Canada), 2019.
- [66] M. van Elk, “The left inferior parietal lobe represents stored hand-postures for object use and action prediction,” *Front. Psychol.*, vol. 5, no. APR, pp. 1–12, 2014.
- [67] J. C. Culham, S. L. Danckert, J. F. X. DeSouza, J. S. Gati, R. S. Menon, and M. A. Goodale, “Visually guided grasping produces fMRI activation in dorsal but not ventral stream brain areas,” *Exp. Brain Res.*, vol. 153, no. 2, pp. 180–189, 2003.
- [68] E. L. Mazerolle, S. D. Beyea, J. R. Gawryluk, K. D. Brewer, C. V Bowen, and R. C. D’Arcy, “White matter fMRI activation in the internal capsule : Co-localization with DTI tractography,” *Neuroimage*, 2010.

- [69] J. M. Soares *et al.*, “A Hitchhiker’s guide to functional magnetic resonance imaging,” *Front. Neurosci.*, vol. 10, no. November, 2016.
- [70] W. K. Kirchner, “Age differences in short-term retention of rapidly changing information,” *J. Exp. Psychol.*, vol. 55, no. 4, pp. 352–358, Apr. 1958.
- [71] J. R. Stroop, “Studies of interference in serial verbal reactions.,” *J. Exp. Psychol. Gen.*, vol. 121, no. 1, pp. 15–23, 1935.
- [72] W. Schneider, D. C. Noll, and J. D. Cohen, “Functional topographic mapping of the cortical ribbon in human vision with conventional MRI scanners,” *Nature*, vol. 365, no. 6442, pp. 150–153, 1993.
- [73] A. Triesman and G. Gelade, “A feature-integration theory of attention,” *Cogn. Psychol.*, vol. 12, no. 1, pp. 97–136, 1980.
- [74] K. K. Zakzanisa, R. Mraz, and S. Graham, “An fMRI study of the Trail Making Test,” *Neuropsychologia*, vol. 43, no. 13, pp. 1878–1886, 2005.
- [75] “Pearson’s Correlation Coefficient - Statistics Solutions.” [Online]. Available: <https://www.statisticssolutions.com/pearsons-correlation-coefficient/>. [Accessed: 13-Jan-2020].

## **Appendix A.**

### **Functional Task**

#### **A.1 Task Requirements**

While there exists a large variety of fMRI tasks, in order to fulfill the purpose of this research there were several limiting specifications. First, the task was required to be completed with both the dominant and non dominant hand, however, it needed to incorporate skills common to the dominant hand and largely unused in the non dominant hand. This was so that there was an intra-participant baseline comparison for training. Therefore, it was expected that there would be significant improvement in the participants left hand after training and a smaller effect in the right hand.

The difficulty of the fine motor task had to be such that it was able to elicit a learning effect over a short training period. The tasks also had to be adaptable for in-scanner completion and at-home training. Finally, the task needed to have a measurable quantification of performance.

#### **A.2 fMRI Task Review**

In order to develop an appropriate task to meet the aforementioned requirements, a review of the common existing tasks was completed. Activation elicited from task-based fMRI is used to investigate a broad range of topics including language, motor, attention, cognition, visuo-spatial orientation, and memory. Many different fMRI tasks have been developed to explore brain function across these systems. A few common examples of fMRI task paradigms are outlined below, though this is by no means a comprehensive list.

Many cognitive fMRI tasks have been adopted from psychological investigations in behavioural performance in order to study brain activity. Two such examples are the n-back memory task and the Stroop task.

Working memory is often studied using the N-back paradigm. In this task, participants are presented a string of stimuli one at a time (commonly letters or patterns of coloured

dots). The participants are expected to identify matching stimuli “n-back” i.e. matching stimuli presented to a stimuli n stimuli back in the sequence [70].

The Stroop paradigm presents participants with names of colours. The colour that the name is printed in can either match the name of the colour or it may not. The participants are asked to identify the name of the colour, irrespective of the colour it is printed in [71].

The most common paradigm for studying motor systems within an MRI scanner is by asking the participants to complete a finger tapping task. These paradigms often have the participant complete a specific sequence of finger to thumb tapping [28], [40].

Presentation of a flashing checkerboard pattern, often presented to only one side of the visual field at a time, is an example of a common visual paradigm. This type of task does not require any response from the participant [72].

An example of a visual task that does require a response would be the visual search paradigm. This task requires the participant to identify a specific target among a number of features. Typically, the speed at which the participant identifies the presence of the target feature is recorded as the behavioural component [73].

The oddball paradigm is a common example of an auditory task that does not require an active participant response. The oddball paradigm presents the participants with a series of tones, most of which are the same volume and frequency. The “oddball” tones are the infrequent tones presented at a different pitch.

The verb generation task, a type of language paradigm, ask the participant to think of an appropriate verb to match given noun (ex. Noun: “Ball”, Verb: “Bounce”).

Many of these tasks do not completely isolate a single system and make require several brain systems working together such as visuo-motor tasks.

The Trail Making Task, having been adapted for completion in the MRI, has participants sequentially connecting numbers (1-2-3 etc.), or a combination of letters and numbers (1-A-2-B etc.). This task integrates many systems such as visual and motor systems, sequencing, and attention [74].

Tasks that require the coordination of systems across hemispheres are known as interhemispheric transfer tasks. These tasks have been shown to drive WM activation, primarily across the corpus callosum (typically in the splenium) [26].

The Poffenberger paradigm is one such task where lateralized visual stimuli are presented ipsi- and contralateral motor reaction responses are recorded. When the visual stimulus presentation is contralateral to the motor response, neural communication is driven between hemispheres [61].

There exists many other tasks used during fMRI scans and these tasks are often adapted or modified to suit the needs of each specific study. With a better understanding of the existing tasks used in fMRI studies a novel motor training task was developed.

### **A.3 Task Development**

A two-week motor training experiment was developed, similar in design as Reid et al. (2017) [28] and Sale et al. (2017) [40]. The motor training block task paradigm for the fMRI scans were developed in MATLAB 2019 with the Psychtoolbox3 package. The purpose was to design a sufficiently complex task that could be completed in the MRI scanner and would elicit a significant learning effect. By creating a task that applied existing translatable skills from one's dominant hand, but not the non-dominant hand created a valuable reference for longitudinal motor learning monitoring.

As a result, two visuo-motor tasks were developed using the same visual stimulus for training precision and speed of hand movements. The tasks were adapted for use in the scanner, as well as for the participants to train at home with every attempt made to be as similar as possible across scanning and at-home training.

One of the tasks was a fine motor task (visual display present in figure 20) requiring the participants to trace the presented path on a screen as rapidly and accurately as possible. The paths consisted of sequential boxes on the screen controlled to total length and frequency of turns. Participants were able to view their progress and were not able to proceed with the task until every previous box has been passed over.

The second type of task was a gross motor task (visual display present in figure 21) requiring participants to fill in as many boxes on the screen as possible without trace or order constraints.

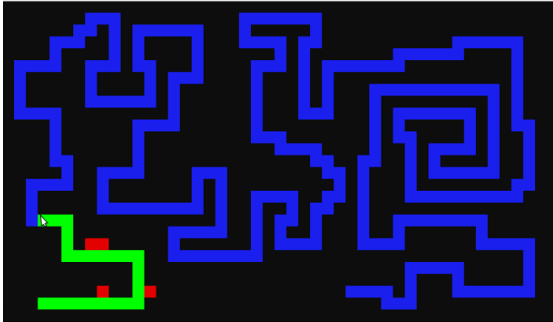


*Figure 20: Screenshot of participant completing the fine motor task*

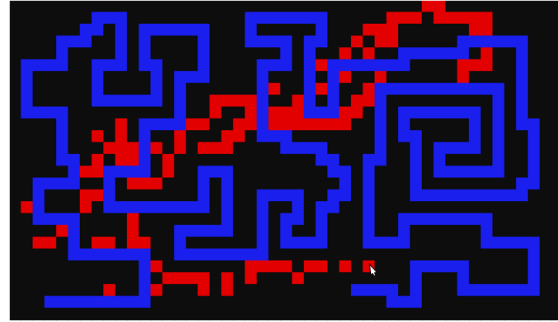


*Figure 21: Screenshot of participant completing the gross motor task*

Once the tasks were programmed, they were piloted both in and outside of the scanner for length, grain, and motion artefact. In order to ensure that the participants were completing the task for the entirety of the on blocks, the trails had to be longer than anyone could feasibly complete in 24 seconds. Motion artefact was also a concern given the coordinated movement of hand and line of sight, however, pilot tests showed that head movement was within the acceptable standard (absolute movement of less than 2mm and less than 2° of rotation).

Both tasks were completed with the participants non-dominant hand and dominant hand as a control. This meant there were four unique conditions:

1. Left hand fine motor task
2. Right hand fine motor task
3. Left hand gross motor task
4. Right hand gross motor task

The scan order of these four conditions was randomized. During training, hand order was also randomized.

The tasks were presented in a jittered block design with 24 second on blocks and rest blocks where a fixation cross was presented. The rest blocks averaged 24 seconds long. An example of the stimulus presentation and corresponding response is presented in figure 20. Each condition had 15 blocks, meaning scan time for one condition was 6

minutes long. For each participant, the trails presented were unique each time to prevent any learning effect specific to one trail. The order of presentation of trails was randomized. For the fine motor task, at the beginning of each on block the mouse would spawn at the beginning of the trail to prevent any initial delay in beginning tracing.

In the scanner the participants used an MRI compatible mouse to complete the tasks. At home training was completed on personal laptops with a standard computer mouse. The visual stimulus presented on the screens and the timing were the same across training and scanning.

Participant score metrics for the fine motor task were dependent on 2 factors: 1) The distance along the trace reach during each 24 second on block and 2) the number of errors (i.e. number of blocks passed over outside of the trace path).

$$Score = \frac{Distance-Errors}{300} * 100 \quad (1)$$

For the fine motor task, score was represented as a percentage of trail completion with an error penalty.

## Appendix B.

### Behavioural Analysis

The details of the behavioural analysis can be found in Grajauskas 2019 [65]. However, a summary of analysis is included for completeness. The effect of training type (fine motor or gross motor task) on average score was investigated using a two-way repeat measure ANOVA. The two factors used in this analysis were hand (dominant and non dominant) and training type (fine motor or gross motor training).

It was found that there was no interaction between hand and training type or significant effect of training type. Therefore, the change in score between baseline and endpoint was investigated using a two-way repeat measure ANOVA. The two factors used in this analysis were hand (dominant and non dominant) and timepoint (baseline and endpoint). Training order (i.e. group number) was set as the between subject factor. The ANOVAs were corrected for multiple comparisons and used conservative degrees of freedom.

Post hoc t-tests (pairwise, two-tailed) were run to investigate score differences as a result of hand. The difference between each corresponding score was calculated. For example: Participant 1 Right Hand Score at Endpoint from Participant 1 Right Hand Score at Baseline.

Detailed results of the behavioural analysis can be found in Grajauskas 2019 [65].

Relevant findings have been summarized as follows.

No interaction was found between training type and hand. No significant main effect was found for training type.

The subsequent analysis found no interactions between hand, timepoint, and training order. However, a significant main effect was found for timepoint and hand.

Difference in scores for the right hand were found not to be significantly greater than 0 ( $p > 0.05$ ) for endpoint > baseline. However, difference in scores for the left hand were found to be significantly greater than 0 ( $t = 3.453$ ,  $p = 0.005$ ) between endpoint > baseline. Therefore, a significant motor learning effect was found for the left hand only. Due to the short training period the dominant hand still scored higher on average (Left hand endpoint score average 13, Right hand endpoint score average 22).

## Appendix C.

### Participant Principal Eigenvector DTI & FCT Overlay

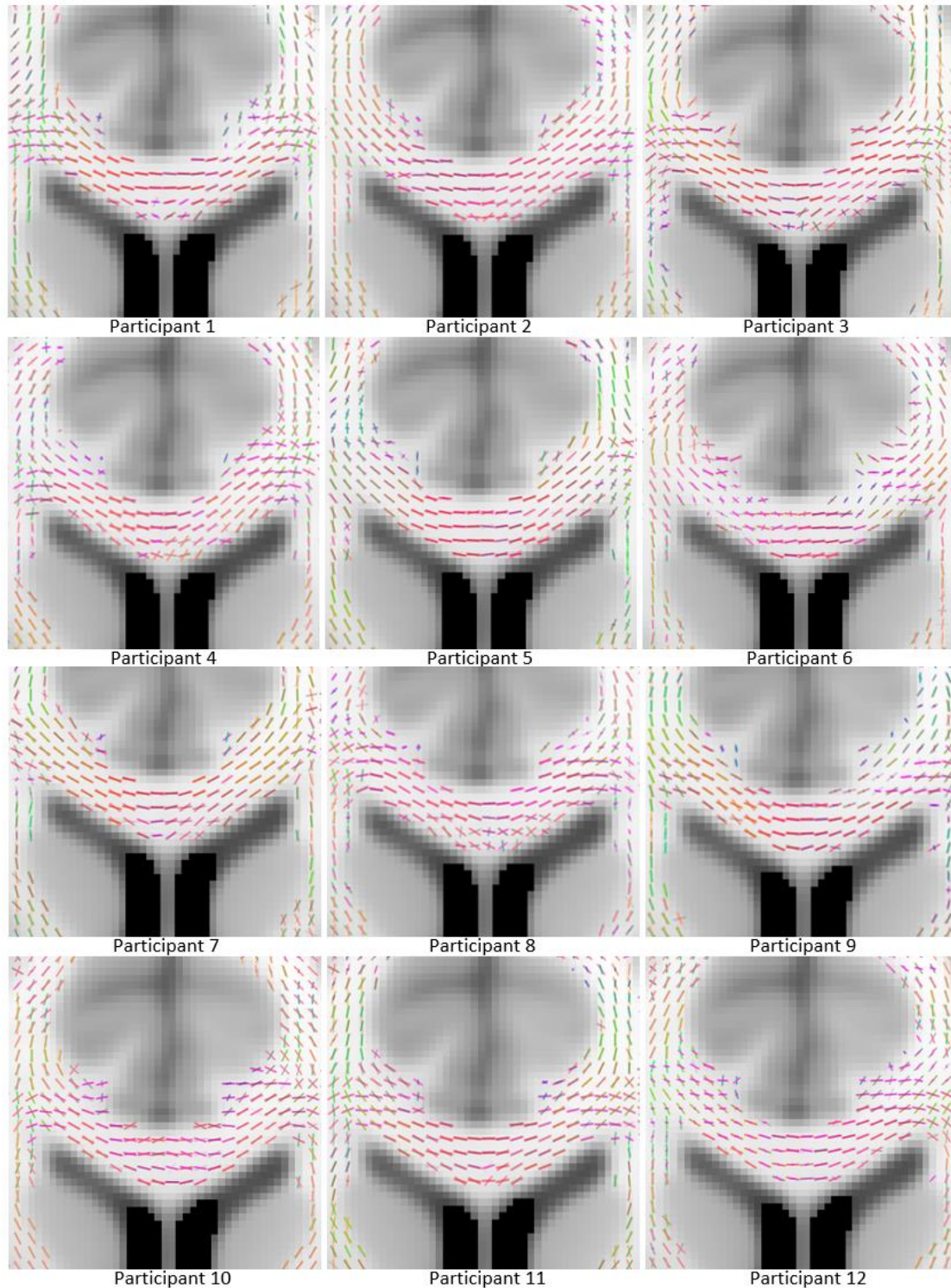


Figure 22: DTI and FCT principal eigenvector masked to WM for all participants at baseline

## Appendix D.

### DTI and FCT 3D Spatial Correlation

In order to investigate if the strength of correlation was localized to certain areas, a map of the spatial correlation between each individuals FCT FA and DTI FA was computed. This correlation was computed between each participants DTI and fMRI scan for both baseline and endpoint (i.e. 24 structural scans and 24 functional scans). For each voxel in the 3D brain space, the Pearson's correlation was computed between a vector of all voxel intensities for FCT FA with DTI FA. The resulting 3D map highlighted areas of high correlation between functional FA and structural FA. To find the areas of highest correlation, the map of Pearson's correlation coefficients was thresholded at 0.5. The resulting 3D spatial correlation map was thresholded at  $R > 0.5$  and cluster size greater than 100 voxels. There are no standards for what makes a good Pearson's correlation value, as these thresholds are data dependent. Therefore, a conservative threshold of 0.5 was used as this is typically regarded as "high correlation" [75].

0 indicated no correlation, any negative value indicates inverse correlation, and positive values between 0 and 1 indicate strength of correlation with a value of 1 being perfectly identical between structure and function.

The DTI and FCT FA maps were masked to the same size in order to carry out the comparison. This masking resulted in the loss of a lot of cortical tissue due to the GM erosion preprocessing step for tract based spatial statistics.

There were no cluster forming statistics computed for this analysis, however, clusters were thresholded to be greater than 100 voxels. These clusters indicated larger areas of high correlation between FCT FA and DTI FA maps for participants.

The table below shows the probable atlas regions based on the Juelich Histological Atlas and the Harvard-Oxford Cortical Structural Atlas. One cluster was excluded from the table for having no atlas region probability greater than 50%.

*Table 5: Regions of high DTI FA (structural) and FCT FA (functional) correlation*

# of Voxels	R max	x location	y location	z location	Atlas Region
424	0.754	72	74	110	Right Cerebral White Matter
255	0.788	88	109	123	GM Primary Motor Cortex
230	0.752	104	65	89	Precuneus
124	0.769	132	72	96	Angular Gyrus
123	0.756	138	73	86	Middle Temporal Gyrus
115	0.831	101	79	119	Left Cerebral White Matter
114	0.725	89	135	124	GM Premotor Cortex
110	0.682	43	96	78	Right Cerebral White Matter

A mix of GM and WM regions were found, showing that strong structural correlation is present regardless of tissue type. Figures 23-26 show some examples of the regions of highest correlation.

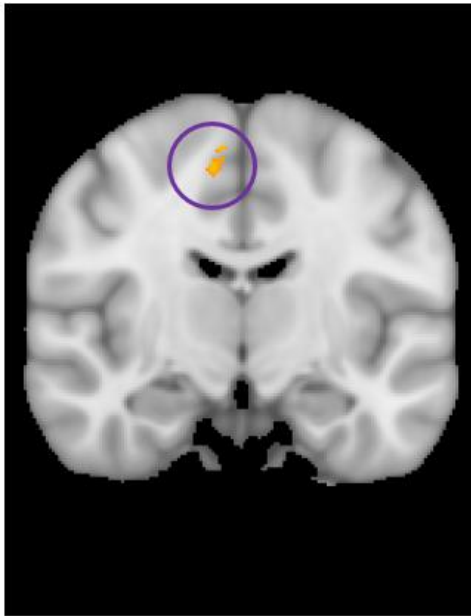


*Figure 23: Primary motor cortex (GM) correlation cluster. Region for motor control.*

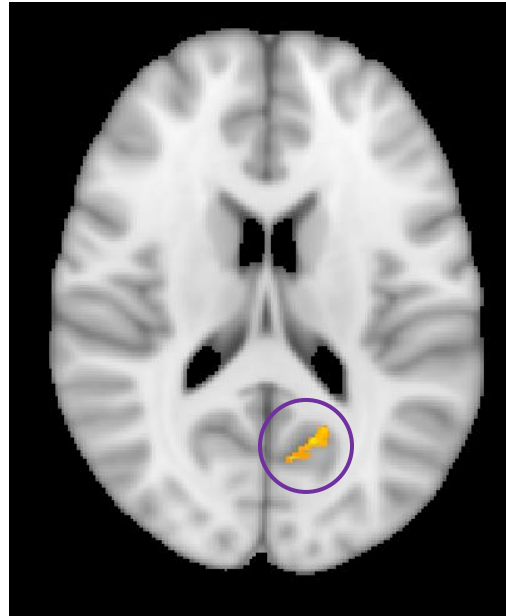


*Figure 24: Precuneus (GM) Correlation Cluster. Region for visuospatial processing and motor coordination*

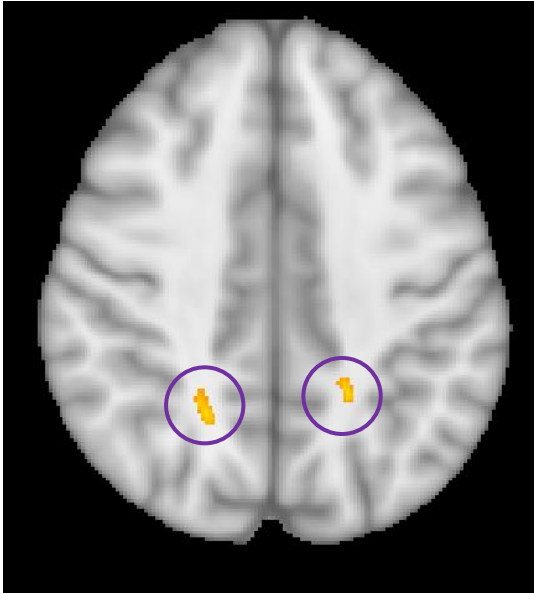


*Figure 25: Primary motor cortex (GM) correlation cluster. Region for motor control.*

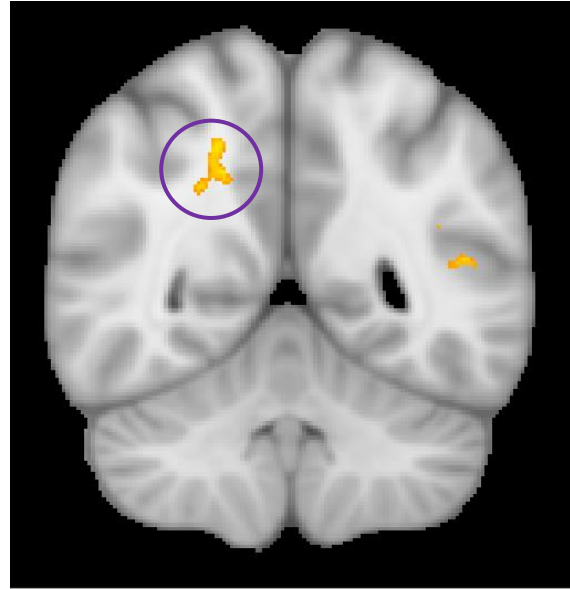


*Figure 26: Precuneus (GM) Correlation Cluster. Region for visuospatial processing and motor coordination*

The 3D correlation analysis detected many larger clusters of correlation in motor areas as well as clusters in regions with secondary visual and motor functions. For example, the angular gyrus plays a role in visuospatial attention and finger recognition and the precuneus is responsible for a number of complex functions such as visuospatial processing and motor coordination. In areas without a strong BOLD signal the meaningfulness of the resulting FCT FA maps may be diminished while areas of expected high BOLD activation it follows that the resulting spatio-temporal correlation of the signal is more accurate and therefore better correlated with the underlying brain structure. However, due to the variance in location of clusters and the lack of accepted thresholds in literature for this type of analysis, it is difficult to draw any conclusive interpretation. Additionally, due to the GM erosion in the tract based spatial statistics preprocessing steps of the DTI and FCT data there is a great deal of information missing from cortical areas.

## Appendix E.

### Additional Figures

#### E.1 Individual Pearson's Correlation

Pearson's correlation between DTI FA and FCT FA maps are reported in Chapter 2. In figure 27 below the Pearson's correlation coefficient for each acquired fMRI scan with the corresponding DTI scan is reported.

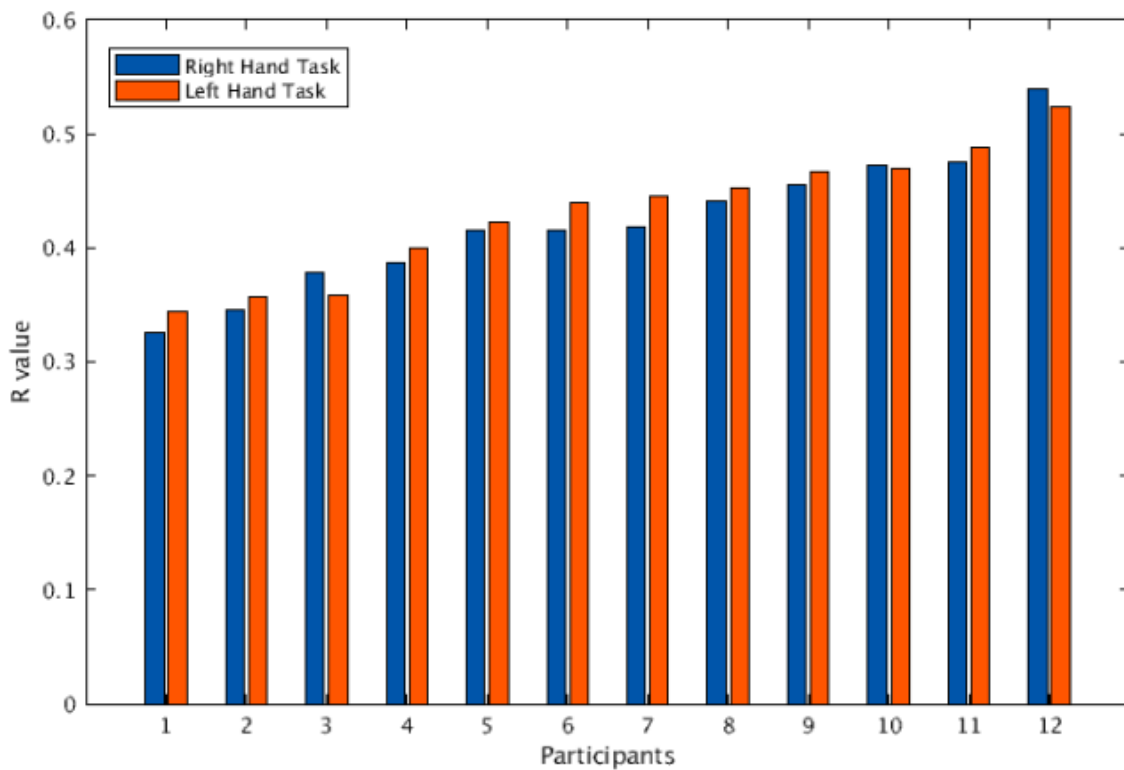


Figure 27: Individual R-values for FCT FA maps compared to participant DTI FA maps for both the right and left hand.

## E.2 Significant Voxel Timeseries Data

Cluster masks of significant voxels in the corpus callosum and superior corona radiata were generated using FSL's cluster function from the preprocessed fMRI data for the left-hand task. The BOLD timeseries data were averages across the masked regions and the data were windowed around the stimulus presentation. Signal means were subtracted from the data and the group averaged timeseries data were plotted for baseline and endpoint scans for each region of interest. Unlike the timeseries data for the internal capsule in section 1.7, this data have not been spatially smoothed resulting in a lower SNR as the BOLD fMRI data were preprocessed with FCT analysis as the primary objective.

The underlying group timeseries data from the significant cluster in the corpus callosum is present in the figure 28 below. Both the baseline and endpoint mean subtracted BOLD data are present here.

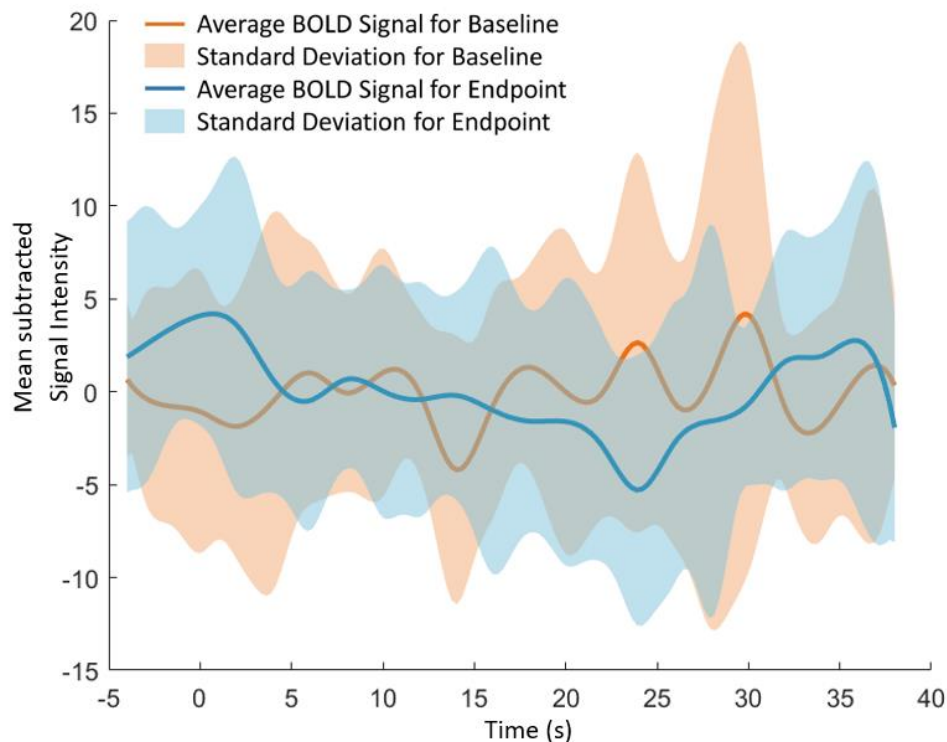
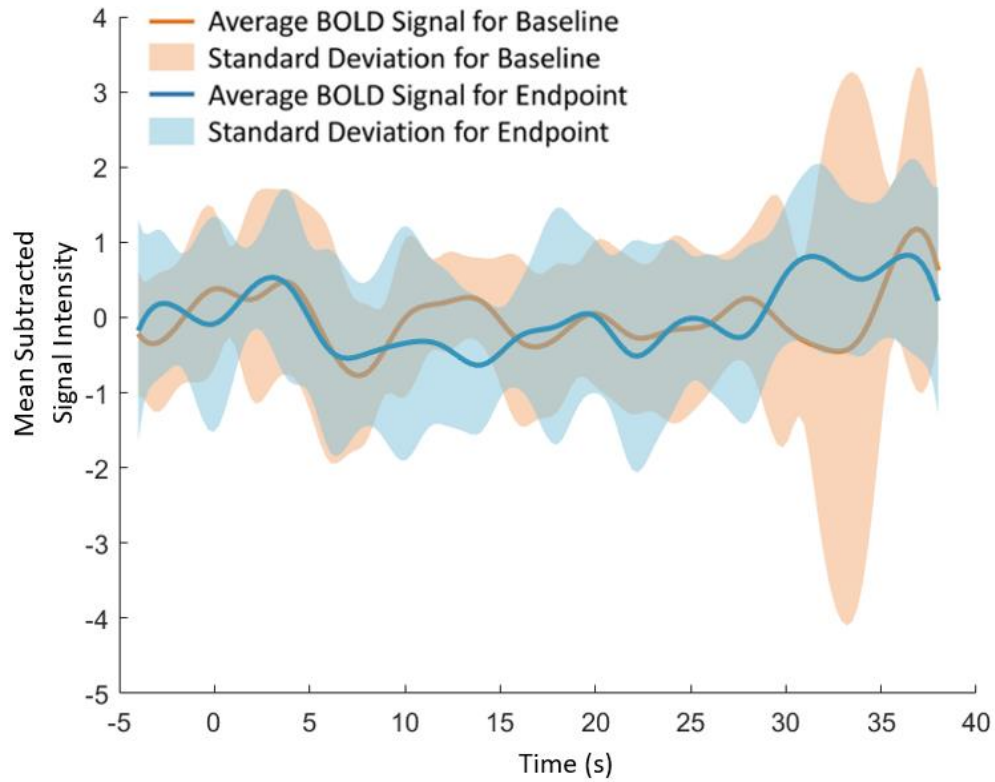


Figure 28: Average across significant corpus callosum voxels with subtracted mean BOLD signal intensity for baseline (orange) and endpoint (blue). Group level standard deviation plotted around timepoint BOLD signal intensity means. Time at zero seconds represents the stimulus onset time.

The underlying group timeseries data from the significant cluster in the superior corona radiata is present in the figure 29 below. Again, both the baseline and endpoint mean subtracted BOLD data are present in this figure.



*Figure 29: Average across significant superior corona radiata voxels with subtracted mean BOLD signal intensity for baseline (orange) and endpoint (blue). Group level standard deviation plotted around timepoint BOLD signal intensity means. Time at zero seconds represents the stimulus onset time.*